Title: Coupling between the TRPC3 ion channel and the NCX1 transporter contributed to VEGF – induced ERK1/2 activation and angiogenesis in human primary endothelial cells.

Running title: TRPC3 in VEGF- induced ERK1/2 activation and angiogenesis

Authors: Andrikopoulos Petros[1,2], Suzanne A. Eccles[3], Muhammad M Yaqoob[1,2]

[1]Diabetic Kidney Disease Centre, Renal Unit, Barts Health NHS Trust, The Royal London Hospital, Whitechapel Road, London E1 1BB, UK

[2]Translational Medicine and Therapeutics, William Harvey Research Institute, Barts and the London School of Medicine, Queen Mary's University of London, London EC1M 6BQ, UK

[3]Division of Cancer Therapeutics, The Institute of Cancer Research, London SW7 3RP, UK

Keywords: VEGF, Endothelium, TRPC3, sodium/calcium exchange, extracellular-signal-regulated kinase (ERK), angiogenesis.

Corresponding Author: Dr. Petros Andrikopoulos, Diabetic Kidney Disease Centre, Translational Medicine and Therapeutics, William Harvey Research Institute, Barts and the London School of Medicine, Queen Mary's University of London, London EC1M 6BQ, UK, Tel.: 44-20-7882-2122, Fax: 44-20-7882-8252, E-mail: p.andrikopoulos@qmul.ac.uk.

ABSTRACT

It has been previously demonstrated that the bi-directional transporter Na^+/Ca^{2+} exchanger (NCX) working in the reverse (Ca^{2+}-influx) - mode promotes the activation of ERK1/2 in response to the key pro-angiogenic cytokine VEGF in human endothelial cells (ECs). However, the molecular event(s) that elicit NCX reversal in VEGF-stimulated ECs remain unclear. Here we investigated whether Na^+ influx via the diacylglycerol (DAG) – activated non-selective cation channel TRPC3 was functionally associated with NCX and whether its activity was required for VEGF-induced ERK1/2 activation and angiogenesis. We provide evidence that TRPC3 inhibitors and siRNA attenuated ERK1/2 phosphorylation, reduced PKCα activity and partially suppressed Ca^{2+} transients in response to VEGF. Additionally, TRPC3 inhibitors and siRNA significantly suppressed endothelial tubular differentiation, an *in vitro* indicator of angiogenesis. We also report that simulating PLCγ activation downstream of VEGF receptor 2 by application of the cell-permeable DAG analogue 1-Oleoyl-2-acetyl-sn-glycerol (OAG) was sufficient to activate ERK1/2 and enhance tubular differentiation. OAG-induced ERK1/2 activation and tubulogenesis were significantly suppressed by TRPC3 and reverse-mode NCX inhibitors and siRNA. Moreover, whilst both reverse-mode NCX and TRPC3 inhibitors attenuated OAG-induced Ca^{2+} transients, only TRPC3 antagonists blunted Na^+ influx in response to OAG. Importantly, when Na^+ was increased in ECs by inhibiting the Na^+-K^+-ATPase, TRPC3 activity was dispensable for OAG-induced ERK1/2 phosphorylation.

Collectively, our research suggests that DAG generation downstream of VEGF receptors activatesTRPC3 causing Na^+ influx with subsequent reversal of NCX, ERK1/2 activation and ultimately contributes to enhanced angiogenesis. Targeting reverse-mode NCX and its upstream initiator TRPC3 could be clinically relevant in conditions characterised by abnormal VEGF signalling.

ABBREVIATIONS

BAPTA-AM: 1,2-Bis(2-aminophenoxy)ethane-N,N,N′,N′-tetraacetic acid tetrakis(acetoxymethyl ester)
CRAC: Ca^{2+}-Release Activated Ca^{2+} Channel
$[Ca^{2+}]_i$: Cytosolic Ca^{2+} concentration
DAG: Diacylglycerol
EC: Endothelial Cell
eNOS: Endothelial Nitric Oxide Synthase
ERK1/2: Extracellular Regulated Kinase 1/2
ECM: Extracellular Matrix Components
GPCRs: G-protein coupled receptors
MAPKs: Mitogen-Activated Protein Kinases
miRNA: micro RNA
NCX: Na^+/Ca^{2+} exchanger
OAG: 1-oleoyl-2-acetyl-sn-glycerol
PI3K: Phosphoinositol-3-kinase
PKC: Protein Kinase C
PLCγ1: Phospholipase Cγ1
PMA: Phorbol 12-myristate 13-acetate
PMCA: Plasma membrane Ca^{2+} ATPase
RTKs: Receptor Tyrosine Kinases
siRNA: Short-interfering RNA
TG: Thapsigargin
SERCA: Sarcoendoplasmic Reticulum Ca^{2+}-ATPase
TREK: TWIK – related K^+ channels
TRPC3: Transient Receptor Potential Canonical 3
VEGF: Vascular Endothelial Growth Factor
VGCCs: Voltage-Gated Ca^{2+} Channels
VGSCs: Voltage-Gated Na^+ Channels

1. Introduction

Dysregulated angiogenesis is detrimentally involved in the progression of many pathophysiological conditions including, but not limited to, diabetic retinopathy, atherosclerosis and aggressive tumour growth [1], [2].

Vascular endothelial growth factor-A (VEGF thereafter), the best studied and most prominent pro-angiogenic cytokine is necessary for endothelial cell (EC) survival under physiological conditions. Abnormal VEGF signalling has also been implicated in the excessive neo-angiogenesis associated with the progression of numerous diseases

including neoplastic expansion and dissemination [1], [2]. Therapeutic strategies targeting the VEGF signalling axis have been approved for a number of malignancies [2]. However, despite the enormous progress in understanding angiogenesis in preclinical tumour models, clinical response to anti-angiogenic therapy is variable and patients generally relapse within a year [3], [4]. Better understanding of endothelial VEGF signalling could therefore potentially improve clinical outcomes.

In adults, VEGF primarily signals by binding to endothelial VEGFR2 (KDR/Flk1) receptors leading to receptor dimerization and VEGFR2 activation via trans-tyrosine autophosphorylation [5]. The subsequent activation of signalling cascades involving phosphoinositol-3-kinase (PI3K), Src kinase and phospholipase Cγ1 (PLCγ1)[5] reprograms the endothelium for angiogenesis by facilitating the complex interaction of downstream effectors such as endothelial nitric oxide synthase (eNOS), protein kinases C (PKCs) and mitogen-activated protein kinases (MAPKs) [5].

The extracellular regulated kinases 1 and 2 (ERK1/2) MAPKs, activated downstream of VEGFR2 in a PKC - dependent manner [6] have been shown to regulate the angiogenic response by controlling EC permeability [7], tubular differentiation [8] and more recently micro RNA (miRNA) expression [9].

VEGF-activated ECs also demonstrate a biphasic increase in cytosolic Ca^{2+} concentration ($[Ca^{2+}]_i$) comprising an initial transient phase, attributed to Ca^{2+} release from internal stores, followed by a sustained influx of Ca^{2+} from the extracellular milieu [10], [11], [12]. Targeting Ca^{2+} signalling in EC is emerging as a viable alternative strategy to VEGF receptor inhibition in controlling dysregulated angiogenesis and tumour vascularisation [13]. In particular, Ca^{2+} influx through the canonical transient receptor potential channels TRPC6 [14], [15], [16], TRPC3 [17] and the pore-forming subunit of the Ca^{2+}-release activated Ca^{2+} channel (CRAC), Orai1 [18] have all been implicated in VEGF-induced angiogenesis.

We have also reported that Ca^{2+} influx through the mammalian transporter Na^+/Ca^{2+} exchanger (NCX) contributed to VEGF-induced human umbilical vein EC (HUVEC) angiogenic properties by modulating ERK1/2 activation in a PKC-dependent manner [11]. The mammalian NCX comprises 3 genes (NCX1 to NCX3) and extrudes cytosolic Ca^{2+} in exchange for extracellular Na^+ when operating in the so-called forward mode. Alternatively, depending on transmembrane $[Ca^{2+}]$ and $[Na^+]$ and the membrane potential, they can operate in the reverse-mode extruding Na^+ and leading to Ca^{2+} influx [19]. The primary physiological role of NCX is to maintain a low cytosolic $[Ca^{2+}]$ working in the forward (Ca^{2+}-efflux) mode particularly in excitable cells [19]. Nonetheless, Na^+ overload and/or plasma membrane depolarisation, typified during ischaemia–reperfusion, could lead to the reversal of the exchanger, subsequent Ca^{2+} overload and cellular injury [20]. Active NCX has been

reported in the endothelium [21], [22] and the splice variants of the cardiac isoform NCX1.3 and NCX1.7 are believed to be the predominant NCX species present in ECs [23].

In our previous studies [11] we showed that acute Na^+ loading of HUVECs promoted VEGF-induced ERK1/2 activation and proposed that associated Na^+-influx pathway(s) along with the control of the membrane potential by voltage-gated Na^+ channels (VGSCs) [10], could be reversing NCX into the Ca^{2+}-influx mode in response to VEGF. In the present study we investigated whether one of those Na^+ mechanisms could be the non-selective cation channel TRPC3 which is known to associate with NCX [24] and to control endothelial angiogenesis [17].

2. Materials and Methods

2.1. Materials

Human recombinant VEGF (V5765), 1-Oleoyl-2-acetyl-*sn*-glycerol (OAG; O6754), BAPTA-AM (A1076), Ouabain (O3125), Ionomycin (I0634), Nifedipine (N7634) and Phorbol 12-myristate 13-acetate (PMA; P1585) were from Sigma-Aldrich. Pyr3 (648490), Pyr6 (203891), Pyr10 (648494) and EGTA-AM (324628) were from Merck Millipore. PD98050 (1213), SN-6 (2184) and Gö6983 (2285) were from Tocris. SEA0400 (HY-15515) was from MedChem Express. All other chemicals used in this study were from Sigma-Aldrich unless stated otherwise.

2.2. Cell culture and protein extraction

HUVECs from pooled donors were purchased from TCS Cellworks (ZHC-2102) and were cultured in Human Large Vessel Endothelial Cell Basal Medium containing growth supplement and antibiotics (Amphotericin B/Gentamycin) also from TCS Cellworks (ZHM-2953) as previously described [10], [11], [25]. HUVEC monolayers at approximately 80% confluency were subcultured using TrypLE™ Express enzyme containing phenol red from ThermoFisher Scientific (12605010). In the present study cells between passages 3-9 were used.

For VEGF and OAG stimulation assays, approximately 100,000 cells plated in 35mm x 10mm dishes (Corning®; 353801) were washed twice with PBS and subsequently serum-starved for 1h in a physiological buffer containing 144 mM NaCl, 5.4 mM KCl, 2.5 mM $CaCl_2$, 1 mM $MgCl_2$, 5.6 mM D-glucose, and 5 mM Tris-HCl, pH 7.4, at 37°C. Cells were pre-incubated with inhibitors or vehicle for 30min prior to the addition of VEGF or OAG. HUVECs were challenged with 50ng/ml VEGF or 100µM OAG at 37°C for the times indicated in the Figure legends. The stimulation was terminated by washing HUVECs once with ice-cold PBS and subsequent application of lysis buffer containing 50 mM Tris-HCl, pH 7.4, 150 mM

NaCl, 1 mM EDTA, 1% v/v Triton X-100, 0.5 mM DTT, 1% v/v protease inhibitor mixture (Sigma-Aldrich; P8340), 1 mM NaF, 5 mM bpVphen (Merck Millipore; 203695), 5 μM fenvalerate (Sigma-Aldrich; F1428), 1 mM Na_3VO_4, and 1% v/v phosphatase inhibitor mixtures 2 and 3 (Sigma-Aldrich; P5726 and P0044 respectively). The cell lysate was placed on ice for 10min and then centrifuged at 5000 x g for 10min at 4°C. The supernatant was kept at -80°C until further use. Protein concentration was determined using the Pierce™ bicinchoninic acid assay (BCA) from ThermoFisher Scientific (23225) using bovine serum albumin (BSA) as protein standard.

2.3. Western Blot

Western blotting was performed using the NuPAGE electrophoresis system and buffers (Invitrogen) according to the manufacturer's instructions and protein bands were visualised using ECL™ Prime from GE Healthcare (RPN2232) as we have described previously [10], [11], [25]. The following antibodies were used in the present study: rabbit anti-phospho-p44/p42 ERK1/2 (Thr-202/Tyr-204; 9101), rabbit anti-p44/p42 (total-ERK1/2; 9102), rabbit anti-phospho-PLCγ1 (Tyr783; 2821), rabbit anti-phospho-PKD/PKCμ (Ser744/748; 2054), rabbit anti-Na^+-K^+-ATPase (3010) all from New England Biolabs. Monoclonal anti-PLCγ1 (total-PLCγ1; sc-374467) and monoclonal anti-PKCα (sc-8393) were from Santa Cruz Biotechnology. Rabbit anti-TRPC3 (NBP2-32258) was from Novus Biologicals. Monoclonal anti-NCX1 was from Swant (R3F1) and monoclonal anti-GAPDH (ab8245) was from Abcam Labs. Densitometric quantification of protein levels was achieved by scanning films and determining the optical densities of the bands of interest using ImageJ 1.46r (National Institutes of Health) as we have described previously [11], [25]. The optical densities of the proteins of interest were normalised against the appropriate loading control and fold changes versus the ratio value of the unstimulated control, arbitrarily set as 1, are shown as described previously [11], [25].

2.4. Immunoprecipitation

Immunoprecipitation of NCX1 from HUVECs was achieved as we previously reported [11], [25]. In brief, protein A-agarose beads from Roche Life Science (11-719-408-001) were washed with ice-cold PBS twice and then incubated with 10 μl anti-NCX1 (Swant) antibody for 1h at 4°C. The antibody-conjugated beads were then washed twice with ice-cold PBS and added to the corresponding cell lysates. After overnight incubation at 4°C, beads were washed twice in lysis buffer and once with PBS and complexed proteins were detached by boiling the beads in electrophoresis loading buffer at 95°C for 5min. In the case of the

immunoprecipitation experiment described in Figure 10G the NCX1 antibody was from Cohesion Biosciences (CPA2077) due to unavailability of the antibody from Swant.

2.5. PKCα translocation assay

Translocation of PKCα to the plasma membrane in response to VEGF was determined by isolating crude membrane fractions as we have described previously [10], [11]. Briefly, HUVECs were challenged with 50ng/ml of VEGF for 10min in the presence of TRPC3 inhibitors or vehicle. The cells were scraped off in 1ml of ice-cold Triton X-free lysis buffer, lysed by passing 20 times through a 21-gauge needle and sonicated for 20sec with 1min intervals. All procedures were carried out on ice. The cell suspension was centrifuged for 5min at 5000 x g and the supernatant was diluted with lysis buffer to 10ml total volume. The sample was then placed in the appropriate ultracentrifugation tubes (Beckman) and spun for 1h at 100,000 x g_{av} in a Ti-70 Ti rotor (Beckman). The cytosolic fraction in the supernatant was removed and the whole membrane fraction was re-suspended by repeated pipetting in 75μl western blot loading buffer at 95^{o}C. The purity of cytosolic versus membrane fractions was assessed by western blot for Na^{+}-K^{+}-ATPase or GAPDH as markers membrane or cytosolic markers respectively. PKCα translocation was also determined by western blot. It should be noted that due to extensive dilution of the cell lysate in order to achieve the minimum safety fill volumes of the centrifugation tubes, PKCα levels in the cytosolic fraction could not be determined.

2.6. siRNA Transfection

HUVECs were transfected with ON-TARGETplus SMARTpool siRNA duplexes against TRPC3 (L-006509), NCX1 (L-007620) or non-targeting siRNA (D-001206) from ThermoFisher Scientific, using Oligofectamine^{TM} (12252011, Invitrogen) as the transfectant as we have previously extensively described [10], [11], [25]. The TRPC3 siRNA pool targeted the following sequences: GGAAGGACCUAGGGAAUAC, GGUCUGGGUUCUUGGAAUG, CGGAAGCUCUCCAUGCAAU, GAGCAGACCAUAGCUAUCA. The NCX1 siRNA duplexes targeted the following sequences: GAAAUGUUAUCGUUCCAUA, GCAGAAGCAUCCAGAUAAA, GCAGACGCCUCCAUAGGUA, GUGAGGAUCUGGAAUGAAA and non-targeting siRNA was against these sequences: UAGCGACUAAACACAUCAA, UAAGGCUAUGAAGAGAUAC, AUGUAUUGGCCUGUAUUAG, AUGAACGUGAAUUGCUCAA. NCX1 knockdown was determined from HUVECs plated in T-75 flasks and transfected in parallel. In the experiments where HUVECs were co-transfected with TRPC3 and NCX1 siRNA duplexes the single- transfection samples were also co-transfected with the appropriate amount of non-targeting control siRNA.

2.7. Intracellular Ca^{2+} Measurement Assays

Measurements of $[Ca^{2+}]_i$ were performed using the Fluo-4NW (Molecular Probes™, F36206) fluorescent Ca^{2+} indicator, according to the manufacturer's instructions as we have described previously [10], [11], [25]. HUVECs were plated at a density of approximately $1x10^4$ cell/well into flat clear-bottomed black-walled 96 well plates (Corning®, 3603) in complete HUVEC medium. The next day the medium was removed; HUVECs were washed twice with PBS and loaded with Fluo-4NW at 37°C, in the dark in Hanks' balanced salt solution (HBSS), supplemented with 20 mM HEPES, pH 7.4, in the presence of 2.5mM probenecid in order to facilitate dye retention. Both HBSS and probenecid were provided with the Fluo-4NW kit (Molecular Probes™, F36206). After 45min, equal volumes of HBSS containing inhibitors or vehicle were added to the corresponding wells and HUVECs were incubated for further 15min. Subsequently, the cell plate was transferred to the assay chamber of the FLIPR Tetra High-Throughput Cellular Screening System (Molecular Devices) and the cells were challenged for 10min with either 50ng/ml VEGF or 100μM OAG in HBSS or HBSS and vehicle alone, as appropriate. The contents of the plate were mixed once and the fluorescence intensity emitted by Fluo-4NW (excitation 485nm, emission 525nm) was measured immediately thereafter for every 2sec. Raw fluorescence data at each time point (F) were normalised by dividing them with the average value of background fluorescence (F_o) obtained for each individual well by taking 10 measurements prior to stimulant addition. All treatments were in triplicate and Ca^{2+} responses were assessed concurrently on the same plate

2.8. Intracellular Na^+ Measurement Assays

Intracellular Na^+ was measured in intact HUVECs loaded the fluorescent indicator Asante NaTRIUM Green-2 - AM (ANG-2) from TEFlabs (3502). HUVECs ($1x10^4$/well) plated into flat clear-bottomed black-walled 96 well plates (Corning®, 3603), as for the Ca^{2+} assays, were loaded with 5μM ANG-2 in HBSS (GIBCO, 14025092) containing 0.1% v/v Pluronic® F-127 (Sigma-Aldrich, P2443) at 37°C in the dark. After 45min the loading solution was removed, cells were washed twice with HBSS and then vehicles or drugs in HBSS were added. After a further 15min incubation at 37°C, the plate was transferred into the assay chamber of the FLIPR Tetra High-Throughput Cellular Screening System (Molecular Devices) and OAG at a final concentration of 100μM, or HBSS alone were added to the corresponding wells. After a short mix step changes in ANG-2 fluorescence were monitored immediately every 2sec for a total of 10min with excitation wavelength of 485nm and emission wavelength of 525nm at 37°C. Equal ANG-2 loading for each experimental condition was assured by obtaining an end-point fluorescent reading (E_{xc} 485nm, E_{mm} 525nm) prior stimulation. Fluorescence (F) at

each time point was normalised by the average of 10 background fluorescent readings taken prior to stimulation (F_0), as described for the Ca^{2+} experiments above. All of the experimental conditions were in triplicate and assayed simultaneously.

2.9. Tubulogenesis Assays

HUVEC tubular differentiation on ECM extracts was assessed according to our previous publications [10], [11], [25] with minor modifications. Briefly, 24 well plates were coated with 250µl phenol red-free, growth factor reduced Matrigel™ (BD Biosciences, 356231) for 1h at 37°C. Subsequently, 2.5 x 10^4 HUVECs in phenol red-free Opti-MEM® (GIBCO, 11058021) where applied to each well. Where appropriate, VEGF (50ng/ml final concentration) or OAG (100µM final concentration) along with TRPC3 inhibitors, reverse-mode NCX inhibitors, or vehicle were also added. The cells were then placed in a humidified incubator at 37°C and 5% CO_2 for 16h in the case of VEGF or 4h in the case of OAG. At the end of the experiment bright-field images were captured with an Olympus LX70 microscope from five random fields of view per sample at ×10 magnification. We opted for a much shorter incubation period for the OAG experiments given that it's reported half-life in living cells is 40min [43]. HUVECs transfected with NCX1 or TRPC3 siRNA were plated on Matrigel™ at the same density (2.5x10^4 cells/well) as the inhibitor experiments 48h post-transfection and challenged with VEGF or OAG for 4h as above. Tubule length for each sample was quantified using ImageJ 1.46r (National Institutes of Health) and was expressed as fold of the tubule length of the unstimulated control sample arbitrarily set to 1.

2.10. Statistical analysis

We determined statistical significance using one- or two-way analysis of variance (ANOVA) and Tukey's *post hoc* test with the GraphPad Prism 5 software, as appropriate. Values of $p < 0.05$ were deemed significant. The data are expressed as the means ± S.E

3. RESULTS

3.1. TRPC3 activity is required for VEGF-induced ERK1/2 phosphorylation

First we investigated whether the specific TRPC3 inhibitor Pyr3 [26] inhibited VEGF-induced ERK1/2 phosphorylation, as we have reported for reverse-mode NCX inhibitors and siRNA [11]. VEGF stimulation (50ng/ml) of serum-starved HUVECs led to a substantial increase in ERK1/2 phosphorylation, peaking between 5 to 10 minutes of stimulation and reverting to baseline levels after 30min. Preincubation of cells with the TRPC3 inhibitor Pyr3 (10µM) suppressed VEGF-induced ERK1/2 activation at all time points tested when compared with

the vehicle-treated (0.5% v/v Me_2SO) controls (Fig. 1A). The effect of Pyr3 on ERK1/2 activation was also dose-dependent (Fig. 1B). Serum-starved HUVECs challenged with 50ng/ml VEGF for 10 min exhibited a 14.40 ± 0.71 - fold normalized phospho-ERK1/2 ratio increase versus the untreated control ratio (arbitrarily set to 1). Pretreatment with 1, 3 or 10μM Pyr3 significantly suppressed ERK1/2 activation for all conditions tested to 9.37 ± 1.50, 7.38 ± 0.87 - and 0.84 ± 0.31 - fold of the unstimulated control phospho-ERK1/2 ratio, $p = 0.045$, $p = 0.022$, $p = 0.003$, $n = 3$ for all, respectively (Fig. 1C). Importantly, Pyr3 pretreatment did not affect PLCγ1 phosphorylation at a site (Tyr^{783}) directly phosphorylated by activated VEGFR2 [5], suggesting that TRPC3 inhibition does not affect VEGFR2 activity and indicating that cells under all conditions tested were equally stimulated and viable (Fig 1B and 1C).

In order to further confirm TRPC3 involvement in VEGF-induced ERK1/2 activation, we employed a second TRPC3 inhibitor, Pyr10 [27]. Pyr10 also attenuated VEGF-induced ERK1/2 activation at all time points tested when compared with controls (Fig. 1D). Unlike Pyr3, Pyr10 did not have an effect on ERK1/2 phosphorylation at lower concentrations (1 or 3μM) (Fig. 1E and 1F). Conversely, 10μM Pyr10 suppressed ERK1/2 activation from 16.50 ± 3.71 -fold to 2.07 ± 0.41 – fold of the unstimulated control ratio, arbitrarily set to 1, $p = 0.025$, $n = 3$ (Fig. 1E and 1F). Pretreatment of HUVECs with Pyr10 also did not affect PLCγ1 phosphorylation in response to VEGF, indicating, as in the case of Pyr3, that Pyr10 did not directly influence VEGFR2 activity at any of the tested concentrations (Fig. 1E and 1F) or non-specifically the ability of HUVECs to transduce VEGF signals.

Next we sought to confirm our pharmacological data employing a gene-knockdown strategy. Transfection of HUVECs with TRPC3-targeting siRNA duplexes significantly blunted the observed ERK1/2 activation when compared with cells transfected with control non-targeting siRNA from 20.50 ± 1.69 -fold to 10.09 ± 1.25 -fold of the unstimulated control, $p = 0.004$, $n = 3$ (Fig. 1G and 1H). TRPC3 protein knock down was confirmed by western blot and shown to be approximately 50% of controls at the protein level (Fig. 1G to 1I).

Taken together our results, so far, suggest that TRPC3 activity is vital for ERK1/2 activation by VEGF, as we have previously shown for VGSCs [10] and NCX1 [11], implying that collectively these proteins could be part of a functional signalling complex.

3.2. TRPC3 inhibitors attenuate PKCα activation in response to VEGF

We have previously reported that VGSC and reverse-mode NCX1 activities modulated ERK1/2 phosphorylation by influencing the activity of the Ca^{2+}-sensitive PKC isoform PKCα [10], [11]. Thus, we next investigated whether TRPC3 activity also affected VEGF-induced PKCα activation. PKCμ/PKD is known to be phosphorylated in response to VEGF and to be

required for VEGF-induced ERK1/2 phosphorylation [28]. Moreover, in HUVEC, PKCμ/PKD was phosphorylated at $Ser^{744/748}$ in a PKCα-dependent manner [28]. Thus, initially we monitored PKCμ/PKD phosphorylation at these sites, as a surrogate of PKCα activity in intact VEGF-stimulated HUVECs. PKCμ/PKD phosphorylation significantly increased after 5min of VEGF addition in concert with ERK1/2 activation (Fig. 2A), as we have previously reported [10]. Preincubation of HUVECs with Pyr3 (10μM) significantly decreased phosphorylation of PKCμ/PKD and ERK1/2 (from 4.90 ± 0.07 to 0.66 ± 0.009 - folds of control, $p = 0.011$, $n = 3$ (Fig. 2*B*) and from 17.65 ± 1.35 to 3.11 ± 0.85 – folds of control, $p = 0.010$, $n = 3$ (Fig. 2*C*) respectively). Pyr3 preincubation also significantly suppressed PKCμ/PKD and ERK1/2 phosphorylation after 10 and 15min of VEGF stimulation (Fig. 2A-2C).

Pyr3 has been reported to suppress CRAC-mediated Ca^{2+} influx non-specifically at similar concentrations to those inhibiting TRPC3 [27]. In order to exclude that the observed effect of Pyr3 on ERK1/2 and PKCμ/PKD phosporylation was due to inhibition of CRAC channels we included in our experiments the CRAC channel inhibitor Pyr6 [27]. Preincubation with Pyr6 (10μM) significantly suppressed VEGF-induced ERK1/2 activation from 17.65±1.35 to 10.88±1.90 – normalised fold of the unstimulated control, $p = 0.008$, $n = 3$, albeit with less potency than Pyr3 (Fir. 2A, 2C). Crucially, preincubation with Pyr6 did not significantly affect phospho-PKCμ/PKD levels after 5min and surprisingly significantly increased PKCμ/PKD phosphorylation after 10min and 15min of stimulation with VEGF (Fig. 2A and Fig. 2C), suggesting that unlike Pyr3 its effect on ERK1/2 activation was not via PKCα.

Interestingly, the effect of TRPC3 inhibition on phospho-PKCμ appears to be to some extent temporal in nature. After 15min phospho-PKCμ levels, although still significantly suppressed, are less decreased when compared to the 5min samples (Fig. 2A and Fig. 2B). A number of PKC isoforms can phosphorylate PKCμ and in addition to PKCα, PKCβ2 and PKCδ are reportedly activated by VEGF [28], [29]. It is plausible that at a later stage another PKC isoform, possible Ca^{2+} insensitive, could as a feedback mechanism compensate and phosphorylate PKCμ to some extent without affecting ERK1/2. Although this is an interesting that merits investigation the focus of the present study is on the ERK1/2 pathway and investigating this is beyond the scope of our study.

As an additional control, we tested that the pharmacological compounds employed did not inhibit non-specifically the intracellular enzymes that translate the Ca^{2+} signal into ERK1/2 activation. This was achieved by bypassing VEGF receptor-mediated Ca^{2+} influx by stimulating HUVECs with the Ca^{2+} ionophore ionomycin (1μM for 5min), a treatment that we have previously shown resulted in robust ERK1/2 activation [10], [25]. Preincubation of HUVECs with the maximum concentrations of Pyr3 (10μM) or Pyr10 (10μM) we have

employed in our study did not have an apparent effect on ionomycin-induced ERK1/2 activation (Fig. 2D), suggesting that their effect was primarily on Ca^{2+} influx. Moreover, this experiment also indicated that treatment of HUVECs with Pyr3 or Pyr10 did not affect their ability to activate ERK1/2 non-specifically by for example affecting their viability. Conversely, 10μM Pyr6 had an observable impact on ERK1/2 activation in response to ionomycin (Fig. 2D). This indicated that the Pyr6 effect on ERK1/2 phosphorylation was probably not Ca^{2+}-influx mediated and possibly non-specific.

We further investigated PKCα activation in VEGF-stimulated HUVECs by monitoring its translocation to the plasma membrane, a process that correlates with activity [29]. Crude membranes and cytosolic fractions of VEGF-stimulated HUVECs in the presence or absence of TRPC3 inhibitors, as indicated, were separated by ultracentrifugation and the prevalence of PKCα in each fraction was tested by western blot, as previously described [10], [11]. Na^+-K^+-ATPase and GAPDH protein levels served as markers of membrane and cytosolic fractions respectively and confirmed separation of the fractions. VEGF stimulation resulted in a 7.27 ± 0.64 – fold increase of normalised PKCα levels compared with control conditions. Pretreatment with Pyr3 (3μM) or Pyr10 (10μM) resulted in a marked decrease in PKCα translocation to 1.72 ± 0.33 and 2.52 ± 0.47 – fold of the control, $p = 0.002$ and $p = 0.003$ respectively, $n = 3$ for both (Fig. 2E and Fig. 2F).

In order to further confirm that TRPC3 activity is upstream of PKC activation, as our finding in Fig. 2E suggests we stimulated HUVECs with PMA. As we have previously shown [10], PMA application was sufficient to activate ERK1/2 and preincubation with Pyr3 (10μM) or Pyr10 (10μM) did not have an apparent effect on PMA – induced ERK1/2 phosphorylation (Fig. 2G)

Collectively, our results indicate that inhibition of TRPC3 activity suppressed VEGF-induced ERK1/2 activation by modulating PKCα activation, as we have previously reported for NCX [11], further supporting our hypothesis that these proteins are functionally coupled.

3.3. Effect of TRPC3 inhibitors on VEGF-induced Ca^{2+} transients

We next investigated the effect of the TRPC3 inhibitors Pyr3 and Pyr10 on VEGF-induced Ca^{2+} transients. Serum-starved HUVECs stimulated with VEGF exhibited a rapid increase in fluorescence of the intracellular Ca^{2+} indicator Fluo-4NW that peaked at ~80sec, as we have previously reported [10], [11]. Cytosolic steady-state Ca^{2+} levels remained significantly higher than the baseline for the duration of the experiment (250sec; Fig. 3A). Preincubation of HUVECs for 15min with the TRPC3 inhibitors Pyr3 (3μM) or Pyr10 (10μM) prior to VEGF stimulation resulted in a partial decrease in the Ca^{2+} response. In particular, Pyr3 (3μM) and Pyr10 (10μM) suppressed the Ca^{2+} signal in VEGF-stimulated HUVECs, quantified as area

under the curve, from 8.08 ± 0.72 – fold of the unstimulated control (arbitrarily set to 1) to 6.08 ± 0.17 - fold and 5.92 ± 0.16 – fold, $p = 0.027$ and $p = 0.015$ respectively, $n = 3$ in triplicate for all conditions (Fig. 3B).

3.4. Effect of TRPC3 inhibitors and siRNA on HUVEC tubular differentiation

HUVEC tubular differentiation on extracellular matrix components was disrupted by TRPC3 inhibitors in a dose-dependent manner. Pyr3 (3μM) significantly reduced tubule formation in the presence of VEGF from 1.64 ± 0.6 - fold to 0.92 ± 0.010 - fold of the unstimulated control, $p = 0.005$, $n = 3$ in duplicate (arbitrarily set to 1; Fig. 4A and Fig. 4B). In the absence of VEGF, 3μM Pyr3 also reduced tubule length to 0.84 ± 0.05 – fold of the control; however, the effect was not statistically significant. A higher concentration of Pyr3 (10μM) completely abolished HUVEC tubular differentiation both in the presence or absence of VEGF (Fig. 4A and Fig. 4B). Similarly, a second TRPC3 inhibitor, Pyr10 at 3μM or 10μM significantly attenuated EC tubule length from 1.64 ± 0.6 – fold to 1.29 ± 0.04 – fold, $p = 0.025$ and 0.97 ± 0.11 $p = 0.013$ – fold of the unstimulated control respectively, $n = 3$ in duplicate for both (Fig. 4A and Fig. 4B). Pyr10 at 10μM also had a significant effect on HUVEC tubulogenesis at basal levels reducing tubule length to 0.77±0.06 – fold of the unstimulated control, $p = 0.031$, $n = 3$ in duplicate. Interestingly, Pyr10 at a concentration that did not affect ERK1/2 activation in the short-term (up to 30min) signalling assays (3μM; Fig. 1E) significantly inhibited HUVEC tubular differentiation. This is not entirely surprising since the tubular differentiation assays lasted longer (16h) and as such are not directly comparable with the signalling assays.

Targeting TRPC3 expression in HUVECs with siRNA also blunted HUVEC tubular differentiation confirming our pharmacological data. Specifically, VEGF stimulation of HUVECs transfected with control non-targeting siRNA resulted in increased tubule length to 1.54 ± 0.04 – fold of the unstimulated control and knocking down TRPC3 expression suppressed HUVEC tubular differentiation to 0.74 ± 0.08 – fold, $p = 0.004$, $n = 3$ in duplicate (Fig. 4C and Fig. 4D). At basal levels, TRPC3 knockdown also significantly reduced cord formation to 0.45 ± 0.04 – fold of the unstimulated control, $p = 0.003$, $n = 3$ in duplicate.

Taken together our results suggest that TRPC3 activity is required for HUVEC tubular differentiation on extracellular matrix components as others have previously reported for the HUVEC-derived cell line EA.hy926 [17] and as we have shown for NCX [11].

3.5. The cell-permeable DAG analogue OAG activates ERK1/2 in HUVECs in a Ca^{2+}-dependent manner

TRPC3 channels are directly activated by diacylglycerol (DAG) generated through PLC-dependent mechanisms downstream of receptor tyrosine kinases (RTKs) or G-protein coupled receptors (GPCRs) [30], [31]. The effect of DAG on TRPC3 can be mimicked by exogenously applying its cell-permeable analogue 1-oleoyl-2-acetyl-sn-glycerol (OAG) [30]. Thus, in order to further confirm that TRPC3 was implicated in VEGF-induced ERK1/2 activation, we investigated whether the direct activation of TRPC3 by OAG was sufficient to activate ERK1/2 in HUVECs.

Indeed, stimulating HUVECs with OAG (100μM) for 5min was sufficient to robustly induce ERK1/2 phosphorylation (Fig. 5A). Loading HUVECs with the "fast" Ca^{2+} chelator BAPTA-AM suppressed ERK1/2 phosphorylation, suggesting that OAG-induced activation of ERK1/2 was Ca^{2+}-sensitive. Conversely, EGTA-AM, a "slow" Ca^{2+} chelator that binds Ca^{2+} with the same affinity as BAPTA-AM, but does not affect local Ca^{2+} transients within 100nm of the Ca^{2+} source [32] did not have an observable impact on OAG-induced ERK1/2 phosphorylation, as we have reported for VEGF [10]. HUVEC stimulation by OAG in a nominal Ca^{2+}-free physiological medium resulted in a substantial reduction in phospho-ERK1/2 levels compared with controls (Fig. 5B), indicating that Ca^{2+} influx was required for ERK1/2 activation by OAG.

We further tested whether influx of extracellular Ca^{2+}, as opposed to Ca^{2+} release from internal stores was involved in OAG-induced ERK1/2 phosphorylation by using thapsigargin (TG), an inhibitor of the sarcoendoplasmic reticulum Ca^{2+}-ATPase (SERCA). We have previously reported that challenging HUVECs with TG (4μM) resulted in a rapid and robust increase of $[Ca^{2+}]_i$ in the presence of extracellular Ca^{2+}, peaking within 2min and remaining at this level thereafter, due to leak of Ca^{2+} from the ER and subsequent activation of CRAC [11]. As we reported previously [11], TG alone had no effect on the levels of phospho-ERK1/2 irrespective of the presence of Ca^{2+} in the extracellular medium in unstimulated HUVECs (Fig. 5C). In contrast, when OAG (100μM) was added 2min after the application of TG, at the peak of the Ca^{2+} signal [11], ERK1/2 phosphorylation was attenuated in the absence of extracellular Ca^{2+} (Fig. 5C) As shown in Fig. 5B extracellular Ca^{2+} was required for OAG-induced ERK1/2 phosphorylation (Fig. 5C). Thus, similarly to our findings for VEGF [11], influx of extracellular Ca^{2+} (rather than release of Ca^{2+} from the internal stores) appeared to be essential for ERK1/2 phosphorylation by OAG.

As in the case of VEGF-induced ERK1/2 activation, phosphorylation of ERK1/2 in response to OAG required PKC activity, since the broad spectrum PKC inhibitor of classical and novel PKCs (Gö6983) dose-dependently suppressed OAG-induced ERK1/2 activation (Fig. 5D). Thus, OAG application was sufficient to induce ERK1/2 activation in HUVECs and this required Ca^{2+} influx from the extracellular milieu and PKC activity. Moreover, our

experiment with TG suggested, as we reported for VEGF [11], that the Ca^{2+} influx pathway controlling ERK1/2 activation was distinct from CRAC.

3.6. TRPC3 activity is required for OAG-induced ERK1/2 phosphorylation

We next directly tested our hypothesis that OAG-induced ERK1/2 phosphorylation was due to TRPC3 activation. Stimulation of serum-starved HUVECs with OAG (100μM) for 5min resulted in a robust increase of ERK1/2 phosphorylation to 18.91 ± 1.70 - fold of the unstimulated control (Fig. 6A and Fig. 6B), a level comparable with that observed upon VEGF stimulation under similar conditions (Fig. 1C). Preincubation of the cells with the TRPC3 inhibitor Pyr3 significantly attenuated ERK1/2 phosphorylation to 8.05 ± 1.82 – fold, $p = 0.001$ and 2.96 ± 1.03 – fold, $p = 0.001$ of the unstimulated control for 3 and 10μM Pyr3 respectively, $n = 3$ for both (Fig. 6B). Targeting TRPC3 protein expression using siRNA-mediated knockdown also suppressed OAG-induced ERK1/2 activation (Fig. 6C). In particular, OAG-induced ERK1/2 phosphorylation was blunted significantly from 13.01 ± 1.77 – to 6.70 ± 1.10 – fold of unstimulated control, $p = 0.011$, $n = 3$ (Fig. 3D). TRPC3 protein knock-down was assessed with western blot and found to be around 50% (Fig. 6C and Fig. 6E).

In cardiac cells, TRPC3 activity reportedly depolarises the plasma membrane and results in Ca^{2+} influx via voltage-gated Ca^{2+} channels (VGCCs) [33]. Preincubating HUVECs with the VGCC inhibitor nifedipine had no apparent effect on OAG-induced ERK1/2 activation (Fig. 6F). Consequently, we inferred that in HUVECs TRPC3 activity influenced Ca^{2+} influx independently of VGCC activity.

3.7. Reverse-mode NCX activity is required for OAG-induced ERK1/2 phosphorylation

We have previously reported that reverse-mode NCX activity modulates VEGF-induced ERK1/2 activation in a PKCα-dependent manner [11], as shown here for TRPC3. Thus, we next investigated whether reverse-mode NCX was also involved in ERK1/2 phosphorylation in response to OAG, further supporting our implied assumption that NCX and TRPC3 are functionally coupled and operate in concert.

Preincubation of HUVECs with the reverse-mode inhibitor SN-6 (10μM) suppressed OAG-induced ERK1/2 activation in a time-dependent manner (Fig. 7A). Furthermore, a second reverse-mode NCX inhibitor, SEA0400, dose-dependently blunted ERK1/2 phosphorylation in response to OAG (Fig. 7B). Specifically, preincubation of HUVECs with 0.5μM or 1μM SEA0400 significantly reduced OAG-induced ERK1/2 activation from 7.32 ± 0.97 - fold of the unstimulated control (arbitrarily set to 1) to 2.66 ± 0.51, $p = 0.005$ - and 1.03 ± 0.70, $p = 0.001$ - fold respectively, $n = 3$ for both (Fig. 7C). A lower concentration of

SEA0400 (0.1μM) also reduced ERK1/2 phosphorylation to 4.39 ± 1.58- fold of the control but the effect was variable and not statistically significant, $p = 0.22$, $n = 3$ (Fig. 7C).

Knocking-down NCX1 protein expression employing siRNA also attenuated OAG-induced ERK1/2 phosphorylation, thus providing independent support of our pharmacological data (Fig. 7D). In HUVECs loaded with control non-targeting siRNA, OAG increased ERK1/2 activation to 11.27 ± 1.16 – fold of the unstimulated control. The response was significantly attenuated in HUVECs where NCX1 expression was targeted by siRNAs to 6.20 ± 1.03 – fold of the unstimulated control, $p = 0.010$, $n = 3$ (Fig. 7E). NCX1 protein knockdown was confirmed in matching transfection experiments (Fig. 7F) and was approximately 50% at the protein level (Fig. 7G), as previously reported [11], [25].

We then investigated, whether blocking TRPC3 or NCX activities using pharmacological inhibitors affected Ca^{2+} transients in response to OAG. OAG application resulted in a rapid increase in the emitted fluorescence of the Ca^{2+}-sensitive indicator Fluo-4NW, peaking within around 2 min and remaining significantly higher than the control levels for the duration of the experiment (10min; Fig. 7H). Preincubation of HUVECs with the TRPC3 inhibitors Pyr3 (3μM) or Pyr10 (10μM) significantly attenuated the bulk Ca^{2+} response to OAG measured as the area under the curve of the emitted fluorescence for each experimental condition (Fig. 7H and Fig. 7IH). In particular, OAG application increased the Ca^{2+} response to 9.25 ± 1.73 – fold of the control level (arbitrarily set to 1), whilst Pyr3 and Pyr10 significantly blunted the response to 2.98 ± 0.69, $p = 0.022$ – fold and 2.00 ± 0.51, $p = 0.013$ – fold of the control respectively, $n = 3$ in triplicate for all conditions (Fig. 7I). Similar to TRPC3 inhibitors, preincubation with the reverse-mode NCX inhibitors SN-6 (10μM) or SEA0400 (1μM) significantly suppressed the Ca^{2+} signal in OAG-stimulated HUVECs quantified as area under the curve (Fig. 7H and Fig. 7I). SEA0400 and SN-6 suppressed OAG induced Ca^{2+} transients from 9.69 ± 1.00 – fold of unstimulated control (arbitrarily set to 1) to 2.91 ± 0.51, $p = 0.018$ – fold and 3.34 ± 0.35, $p = 0.018$ - fold respectively, $n = 3$ in triplicate (Fig. 7I).

Therefore, taken together, our results suggest that TRPC3 and NCX activities were required for OAG – induced Ca^{2+} signalling, possibly working in concert. .

3.8. TRPC3 activity regulates OAG-induced signalling by modulating Na^+ influx

Given that TRPC3 is a non-selective cation channel and both TRPC3 and NCX activities were required for OAG-induced signalling, we postulated that the effect of TRPC3 could be due to Na^+ influx and subsequent reversal of NCX leading to Ca^{2+} influx. We tested this by monitoring the effects of inhibitors of TRPC3 and reverse-mode NCX on intracellular [Na^+] in response to OAG using the cell permeable fluorescent Na^+ indicator ANG-2. Challenging

HUVECs loaded with ANG-2 with OAG resulted in an increase in the emitted fluorescence that plateaued within approximately 250sec and remained significantly higher than the unstimulated control level for the duration of the experiment (10min; Fig *8*A). Preincubating HUVECs with the reverse-mode NCX inhibitors SN-6 (10μM) or SEA0400 (1μM) modestly increased the bulk Na^+ signal, measured as the area under the curved of the normalised emitted fluorescence from 6.51 ± 0.75 – fold to 7.45 ± 0.55 – fold and 7.39 ± 0.43 – fold of the unstimulated control (arbitrarily set to 1), respectively (Fig. 8B). The effect of reverse-mode NCX inhibitors on [Na^+] was not significant; $p = 0.22$ and $p = 0.26$ respectively, $n = 3$ in triplicate for both. Conversely, preincubation of HUVECs with Pyr3 (3μM) or Pyr10 (10μM) significantly attenuated the Na^+ signal in response to OAG (Fig. 8A). In particular, Pyr3 and Pyr10 suppressed the total Na^+ response, measured as the area under the curve of the emitted ANG-2 fluorescence over time, from 6.51 ± 0.75 – fold of the unstimulated control (set to 1) to 1.83 ± 0.38, $p = 0.021$ - fold and 2.23 ± 0.42, $p = 0.033$ - fold respectively, $n = 3$ in triplicate for both (Fig. 8B).

We next investigated whether acutely loading HUVECs with Na^+ by inhibiting the Na^+-K^+-ATPase with ouabain and thus promoting reverse-mode NCX, augmented OAG-induced ERK1/2 activation, as we reported for VEGF [11] or thrombin stimulation [25]. Preincubation of serum-starved HUVECs with ouabain (100μM for 1min) prior to brief stimulation with OAG (100μM for 2min) significantly enhanced ERK1/2 phosphorylation from 1.83 ± 0.45 – fold of unstimulated control to 6.81 ± 1.07 – fold, $p = 0.014$, $n = 3$ (Fig. 8C and Fig. 8D). The reverse-mode NCX inhibitor SN-6 cancelled out the effect of ouabain on OAG-induced ERK1/2 activation, suggesting that it was probably via induction of reverse-mode NCX (Fig. 8C).

We then tested the effect of the TRPC3 inhibitor Pyr3 (3μM) on OAG-induced ERK1/2 phosphorylation in the presence of ouabain, as described in Fig. 8C. Pretreatment of HUVECs with ouabain enhanced ERK1/2 phosphorylation in response to brief OAG challenge as expected; however, Pyr3, unlike SN-6 (Fig. 8C), had no apparent effect on ERK1/2 activation in the presence of ouabain (Fig. 8E).

Consequently, taken together these experimental data suggest that TRPC3 activity was primarily required for increasing [Na^+] in response to OAG, presumably resulting in Ca^{2+} influx via reverse-mode NCX. Moreover, in HUVECs already loaded with Na^+ (by inhibiting the Na^+-K^+-ATPase with ouabain) TRPC3 activity, unlike NCX activity, was dispensable for OAG-induced ERK1/2 phosphorylation.

3.9. OAG-induced HUVEC tubular differentiation requires TRPC3 and NCX activities

We investigated whether OAG stimulation of HUVECs, similar to VEGF, was sufficient to induce tubular differentiation on extracellular matrix components and whether ERK1/2, TRPC3 and NCX activities were involved. Application of OAG for 4h increased HUVEC tubule length to 1.54 ± 0.04 – fold of the unstimulated control (set to 1; Fig. 9A and Fig. 9B). The reverse-mode NCX inhibitor SEA0400 reduced tubule length from 1.54 ± 0.04 - fold to 1.06 ± 0.05, $p = 0.004$ – fold or 0.91 ± 0.04, $p = 0.001$ – fold of control at 0.5μM or 1μM respectively, $n = 3$ in duplicate for both (Fig. 9*A* and Fig. 9*B*). The TRPC3 inhibitor Pyr3 (3μM) significantly reduced HUVEC tubule length to 0.77 ± 0.07 – fold of the unstimulated control, $p = 0.001$, $n = 3$ in duplicate, whilst 10μM Pyr3 completely abolished the response (Fig. 9A and Fig. 9B). The effect of SEA0400 and Pyr3 was probably due to inhibition of ERK1/2 phosphorylation since an inhibitor of the ERK1/2 pathway (PD98050 at 10μM) also significantly reduced HUVEC normalized tubule length to 0.84 ± 0.05 – fold of the unstimulated control, $p = 0.001$, $n = 3$ in duplicate. SEA0400 (1μM), Pyr3 (3μM) and PD98050 (10μM) also modestly (albeit significantly) suppressed HUVEC tubulogenesis at basal levels to 0.85 ± 0.04, $p = 0.030$, 0.75 ± 0.05, $p = 0.016$, and 0.79 ± 0.09, $p = 0.015$ – fold of the unstimulated control respectively, $n = 3$ in duplicate for all conditions (Fig. 9A and Fig. 9B). A higher concentration of Pyr3 (10μM), as in the case of VEGF stimulation (Figure 4), completely abolished HUVEC tubule formation (Fig. 9A).

Similar results were obtained when NCX1 and TRPC3 expression was targeted with siRNA. In HUVECs transfected with control non-targeting siRNA, OAG enhanced tubule formation to 1.55 ± 0.06 – fold of the unstimulated control whilst with siRNA targeting TRPC3 or NCX1 expression it was significantly reduced to 0.86 ± 0.04, $p = 0.001$ – fold and 1.04 ± 0.5, $p = 0.010$ – fold respectively, $n = 3$ in duplicate for both (Fig. 9C and Fig. 9D). TRPC3 knockdown also significantly suppressed HUVEC tubule formation to 0.66 ± 0.07 – fold in the absence of OAG stimulation, $p = 0.018$, $n = 3$ in duplicate, as we observed for VEGF (Fig. 4D), whilst targeting NCX1 had no significant effect (Fig. 9C and Fig. 9D).

3.10. Simultaneous Inhibition of TRPC3 and NCX1 activities has an additive effect on VEGF - and OAG – induced ERK1/2 activation.

Finally, we directly assessed whether TRPC3 and NCX1 activities had an additive effect on ERK1/2 phosphorylation in response to VEGF, as our work so far suggests and as would have been expected if they work in concert. HUVECs were preincubated with Pyr3 (3μM) or SN-6 (5μM), concentrations we have shown supressed around 50% of VEGF – induced ERK1/2 activation (Fig. 1B and [10] respectively), alone or in combination. As expected, Pyr3 or SN-6 at these concentrations reduced VEGF-induced ERK1/2 activation to around 50% of the control (Fig. 10A and Fig. 10B). Conversely, combining Pyr3 and SN-6 treatments resulted in significant attenuation of ERK1/2 activation in comparison to each

treatment alone. Specifically, combining Pyr3 (3μM) and SN-6 (5μM) reduced normalized ERK1/2 phosphorylation to 2.65 ± 0.20 fold of the unstimulated control from 8.58 ± 0.43, p = 0.02, n = 3; and 8.09 ± 0.26, p = 0.01, n = 3, for each treatment alone (Fig. 10A and Fig. 10B).

Combining Pyr3 and SN-6 treatments similarly to VEGF also had an additive effect in OAG – stimulated HUVECs. Whilst, Pyr3 (3μM) or SN-6 (5μM) pretreatment attenuated OAG – induced ERK1/2 activation by around 50% to 7.10 ± 0.50 – and 6.60 ± 0.79 – fold of control respectively, their combination further suppressed ERK1/2 activation to 1.80 ± 0.49 – fold of control (p = 0.009 and p = 0.011 respectively, n = 3 for both; Fig. 10C and Fig. 10D).

The pharmacological data were also confirmed by combining siRNA treatments targeting TRPC3 and NCX1 gene expression. Knocking down TRPC3 or NCX1 expression with siRNA resulted in around 50% reduction in ERK1/2 phosphorylation as expected (Fig. 1G and [10]). Combining siRNA treatment had a significantly more pronounced effect on VEGF – induced ERK1/2 phosphorylation. Specifically, TRPC3 siRNA reduced ERK1/2 activation to 10.40 ± 0.58 – fold of control, whilst NCX1 siRNA reduced ERK1/2 activation to 10.27±0.48 – fold (Fig. 10E and Fig. 10F). Combining siRNA treatments significantly reduced ERK1/2 phosphorylation further to 4.98 ± 0.34 fold of control (p = 0.006 and p = 0.004 when compared to the single treatments, n = 3 for both; Fig. 10E and Fig. 10F). Knocking down NCX1 did not appear to have an effect on TRPC3 protein expression for the 48h duration of the experiment (Fig. 10E, top panel). Similarly, knocking down TRPC3 did not appear to influence NCX1 protein expression (Fig. 10G). It should be noted that in all conditions HUVECs were transfected with 200nM siRNA in total (See also Section 2.6). Additionally, a different antibody against NCX1 was used in Fig. 10G than the one used for the experiment shown in Fig. 7F (see also Section 2.4.), due to unavailability of the original Antibody from Swant. The new antibody recognised only one NCX1 band, suggesting that the lower molecular weight band observed in Fig. 7F and in our previous work, [10] and [25], possibly corresponded to a proteolytic fragment.

Collectively, since the effect of treatments was additive, this line of investigation supports our hypothesis that TRPC3 and NCX1 work in concert to activate ERK1/2 downstream to VEGF

4. DISCUSSION

TRPC3s are non-selective cation channels that require DAG (generated by PLCs downstream of RTKs and GPCRs) for maximal activity [30], [31]. TRPC3s are known to be expressed in HUVECs [34] and were activated downstream of VEGF when heterologously co-expressed with VEGFR2 in HEK293 cells [14]. Moreover, TRPC3 activity in coronary

arterial EC enhanced monocyte adhesion when challenged with TNFα *in vitro* [35]. Also, in mice where TRPC3 was genetically overexpressed specifically in the endothelium, atherosclerotic lesion sizes were increased [36]. TRPC3 activity has also been directly implicated in tubular differentiation in the HUVEC-derived cell line EA.hy926 [17]. Moreover, TRPC3-mediated Na^+ influx has been shown to result in Ca^{2+} influx indirectly by reversing the bi-directional transporter NCX first in HEK293 cells [24] and later in a number of additional experimental systems, including intact hearts [37], smooth muscle cells [38] and platelets [39]. Nonetheless, despite the well-documented role of TRPC3 in endothelial pathophysiology, precisely how its activity influences downstream signalling remains largely unexplored. Additionally, to the best of our knowledge, coupling between TRPC3 and NCX has not been previously reported in the endothelium. Here, we provide evidence that TRPC3s, downstream of VEGFR2 and PLCγ1, regulates ERK1/2 activation and angiogenesis by modulating PKCα activity, probably in concert with reverse-mode NCX. Furthermore, we demonstrate that direct activation of TRPC3s by the cell-permeable DAG analogue OAG was sufficient to activate ERK1/2 and promote EC tubular differentiation *in vitro* and this also required reverse-mode NCX activity, further supporting our hypothesis that TRPC3s and NCX1 are functionally coupled in HUVECs. More specifically:

4.1. Effect of TRPC3 activity on ERK1/2 activation and $[Ca^{2+}]_i$ transients in response to VEGF

The TRPC3 inhibitors Pyr3 and Pyr10 or TRPC3 protein depletion with siRNA blunted VEGF-induced ERK1/2 activation (Section 3.1.; Fig. 1), as we have previously reported for NCX [11] and VGSCs [10]. Similar to our previous reports [10], [11]. TRPC3 activity was required for PKCα activation in response to VEGF, as exemplified by PKCα translocation to the membrane fraction and PKD/PKCμ phosphorylation (Section 3.2.;.Fig. 2), a process known to precede ERK1/2 activation [28]. The inhibitors of TRPC3 (Pyr3 or Pyr10) also suppressed bulk Ca^{2+} transients in HUVECs challenged with VEGF by approximately 25% (Section 3.3.; Fig. 3), as we have reported with reverse-mode NCX inhibitors [11]. TRPC3 inhibition did not completely abolish the VEGF-induced Ca^{2+} response in HUVECs, however, this is not surprising since a number of receptor – or store - operated channels have been shown to regulate Ca^{2+} influx in ECs [13], [40]. Nonetheless, our results indicate that TRPC3 activity, possibly coupled with reverse-mode NCX [11] conduct at least a significant proportion of the Ca^{2+} signal required for VEGF-induced ERK1/2 activation in a spatially-restricted manner. Additionally, TRPC3 activity was also required for HUVEC tubular differentiation (Section 3.4.; .Fig. 4).

Collectively, our present findings and our previous studies [10], [11], suggest that TRPC3, NCX1 and VGSCs form a functionally coupled signalling complex to modulate

VEGF-induced Ca^{2+} influx, PKCα activation, ERK1/2 phosphorylation and ultimately, HUVEC tubular differentiation. Despite considerable focus on the role of TRPC3 activity and Ca^{2+} influx in pathophysiology, it is often overlooked that TRPC3s are non-selective cation channels. Furthermore, in bovine aortic EC, TRPC3s were roughly equally permeable to Na^+ and Ca^{2+} with a ratio of PCa/PNa≈1.62 [41]. Consequently, since in physiological fluids, similar to our experimental system, extracellular [Na^+] is roughly 60-fold greater than [Ca^{2+}], even taking into account the higher concentration gradient for Ca^{2+} normally found in cells, it can be expected that a substantial amount of Na^+ ions will enter the cell through TRPC3. Indeed, in a number of systems, including HEK293 cells [24], intact hearts [37], smooth muscle cells [38] and platelets [39] TRPC-mediated Na^+ influx was shown to result in Ca^{2+} influx indirectly by reversing NCX. Our findings that TRPC3 activity, like reverse-mode NCX [11], regulated VEGF-induced ERK1/2 and PKCα activation suggest that this is also the case in VEGF-stimulated endothelial cells.

4.2. CRAC currents are not involved in acute VEGF-induced ERK1/2 phosphorylation

The TRPC3 inhibitor Pyr3, used in our experiments, had minimal impact on the activities of other closely related TRPC isoforms [26]. However, Pyr3 reportedly inhibits CRAC currents non-specifically in mast cells with the same potency as TRPC3 activity [27]. In HUVECs, CRAC currents are primarily mediated by the plasma membrane Orai1 and the ER STIM1 subunits of the CRAC channel [40] and Orai1 activity has been implicated in the angiogenic response of HUVECs to VEGF [18]. We further corroborated TRPC3 involvement by including in our experiments a second inhibitor more specific for TRPC3 than CRAC, Pyr10 [27]; and siRNA. Furthermore, others have shown that knocking down Orai1 (the pore-forming constituent of CRAC) had no effect on HUVEC tubular differentiation [17]. Nonetheless, we directly tested the involvement of Ca^{2+} influx by CRAC channels on VEGF-induced ERK1/2 activation by using the CRAC inhibitor Pyr6 that had minimal effect on TRPC3 activity in TRPC3-overexpressing HEK293 cells [27]. Pyr6 suppressed VEGF-induced ERK1/2 activation with less potency than TRPC3 inhibitors without reducing PKD/PKCμ phosphorylation (Section 3.2.; Fig. 2A and Fig. 2C), a surrogate marker of PKCα activity [28]. Moreover, Pyr6, unlike Pyr3 or Pyr10, also inhibited ERK1/2 activation in HUVECs stimulated with the Ca^{2+} ionophore ionomycin (Section 3.2.; Fig. 2D), suggesting that its effect was independent of Ca^{2+} influx and possibly non-specific.

Initiating CRAC with thapsigargin in the presence of extracellular Ca^{2+} did not activate ERK1/2 (Section 3.5.; Fig. 5C). Conversely, application of ionomycin, expected to increase $[Ca^{2+}]_i$ uniformly across the plasma membrane did (Fig. 2D). Additionally, our previously published work suggested that ERK1/2 activation in response to VEGF required

localised Ca^{2+} rise [10]. Thus, it is conceivable that in VEGF-stimulated ECs the CRAC current and the Ca^{2+} signal required for ERK1/2 phosphorylation constitute two functionally and spatially distinct Ca^{2+} microdomains. This is supported by the finding that CRAC-mediated Ca^{2+} influx did not occur uniformly across the plasma membrane of HeLa cells but at "hotspots" where the plasma membrane and the ER are in close proximity [42]. Nevertheless, our work does not conclusively preclude Orai1/CRAC involvement in angiogenesis and VEGF signalling, since long term CRAC inhibition could modulate angiogenesis indirectly by regulating the filling of the internal Ca^{2+} stores.

4.3. The DAG analogue OAG activates ERK1/2 in a TRPC3- and NCX1-dependent manner

The implied functional association of NCX with TRPC3 was further investigated by the application of the cell-permeable DAG analogue OAG. OAG directly activates the TRPC3/TRPC6/TRPC7 subfamily of TRPC channels [30], [31] and in human microvascular ECs it produced non-specific cation currents similar to those activated by VEGF [14].

We report here that OAG on its own was sufficient to substantially elevate phosphoERK1/2 levels in ECs. Our results (Section 3.5.; Fig. 5A-C), suggest, as we have reported for VEGF [10], that local Ca^{2+} influx as opposed to global Ca^{2+} is required for this. Moreover, our experimental data using a nominal Ca^{2+}-free physiological medium (Section 3.5.; Fig. 5B), or thapsigargin (Fig. 5C). similar to our previous report for VEGF [11], indicate that Ca^{2+} influx rather than Ca^{2+} release from the internal stores was critical for OAG-induced ERK1/2 activation. Again, as for VEGF [10], ERK1/2 phosphorylation in response to OAG required PKC activity. Taken together our findings suggest that OAG and VEGF-induced ERK1/2 activation share crucial similarities; particularly their dependence on Ca^{2+} influx and PKC activity and consequently OAG could be used to study aspects of VEGF signalling.

TRPC3 activity was also required for OAG-induced ERK1/2 activation. TRPC3 inhibitors (Section 3.6.; Fig. 6A) or siRNA (Section 3.6.; Fig. 6C) reduced OAG-induced ERK1/2 phosphorylation. In cardiomyocytes Na^{+}-influx via TRPC3 resulted indirectly in Ca^{2+} influx via VGCCs upon plasma membrane depolarisation [33]. This appears not to be the case in ECs, since, as we showed previously for VEGF [10], an inhibitor of VGCCs had no obvious effect on OAG-induced ERK1/2 phosphorylation (Section 3.6.; Fig. 6F).

Our hypothesis that TRPC3 and NCX1 are functionally coupled and regulate ERK1/2 signalling in HUVECs was further validated by our finding that treatment with reverse-mode NCX inhibitors (Section 3.7.; Fig. 7A to Fig. 7C) or NCX1-targeting siRNA (Section 3.7.; Fig. 7D *and* Fig. 7E) also significantly attenuated OAG-induced ERK1/2 phosphorylation, as we have previously shown for VEGF [11]. This was further corroborated by our finding that combining pharmacological inhibitors targeting TRPC3 and NCX1 activities or siRNA

treatments targeting their expression had an additive effect on ERK1/2 activation by VEGF or OAG (Fig. 10).

4.4. Effect of TRPC3 and reverse-mode NCX activities on OAG-induced Ca^{2+} and Na^{+} transients

In platelets activation of DAG-sensitive TRPC channels increased $[Na^{+}]_i$, whilst subsequent Ca^{2+} influx was mediated via reverse-mode NCX [39]. We investigated whether this was also applicable to OAG-stimulated ECs. Indeed, OAG, as previously reported for microvascular ECs [14], significantly increased $[Ca^{2+}]_i$ in HUVECs, whilst pretreatment with both TRPC3 (Fig. 7H) or reverse-mode NCX inhibitors (Fig. 7H), significantly blunted the Ca^{2+} signal, suggesting that TRPC3 and NCX constitute the primary Ca^{2+}-influx routes activated by OAG. Crucially, when we measured intracellular $[Na^{+}]$ under identical conditions, we observed a significant increase in intracellular Na^{+} upon OAG application that was suppressed by TRPC3 inhibitors (Section 3.8.; Fig. 8A). Conversely, in samples pre-treated with reverse-mode NCX inhibitors intracellular $[Na^{+}]$ was marginally, although not statistically significantly, higher than the OAG-treated control (Fig. 8A and Fig. 8B). It is tempting to speculate that this was due to reduced Na^{+} extrusion after inhibition of reverse-mode NCX, however further experimentation is required to support this hypothesis. Even if this is not the case our results clearly demonstrate that reverse-mode NCX activity did not increase intracellular Na^{+}. We further explored the role of intracellular Na^{+} by monitoring ERK1/2 activation in response to OAG in ECs loaded with Na^{+} by briefly inhibiting the Na^{+}-K^{+}-ATPase with ouabain as we did previously for VEGF [11] and thrombin [25]. Ouabain significantly amplified OAG-induced ERK1/2 phosphorylation and the response was blunted by SN-6, signifying that presumably reverse-mode NCX induction by high intracellular Na^{+} was probably involved (Section 3.8.; Fig. 8C). On the contrary, pre-treatment of HUVECs with Pyr3, an inhibitor of TRPC3, had no apparent effect on the enhanced OAG-induced ERK1/2 phosphorylation observed in ouabain-treated cells (Section 3.8.; Fig. 8E). This experiment suggests that once HUVECs are loaded with Na^{+} via another route (inhibition of the Na^{+}-K^{+}-ATPase in this instance) that can promote reverse-mode NCX, then TRPC3 activity is dispensable for OAG-induced ERK1/2 phosphorylation.

Collectively, this line of investigation corroborated our hypothesis that in stimulated HUVECs Na^{+} influx was primarily mediated by TRPC3 whilst Ca^{2+} entry occurred via subsequent induction of reverse-mode NCX. This is supported by our findings that (i) although both TRPC3 and NCX inhibitors suppressed OAG-induced Ca^{2+} influx only TRPC3 inhibitors attenuated Na^{+} transients and (ii) once cells were loaded with Na^{+} TRPC3 activity, (unlike reverse-mode NCX) was superfluous for OAG-induced ERK1/2 activation.

We also attempted to monitor whole-cell intracellular Na^+ in VEGF-stimulated HUVECs. Unlike our experiments with OAG, in this instance we could not detect reliably an increase in intracellular Na^+ since the response was variable and often barely detectable (not shown). Thus, although VEGF-induced Ca^{2+} transients are more prominent than those in response to OAG, the global Na^+ signal appears to be significantly more modest, at least when measured with our experimental setup. This is not entirely surprising, since as discussed in Section 4.1., other Ca^{2+} influx mechanisms also contribute to the global Ca^{2+} transients observed in response to VEGF. Interestingly, reverse-mode NCX [11] and TRPC3 inhibitors (Fig.3A and Fig. 3B) both suppressed approximately 20% of the total VEGF-induced Ca^{2+} signal. This is comparable to the global Ca^{2+} signal (approximately 25% increase from baseline) we observed in response to OAG (Fig. 7H). Notably, in both cases, despite the difference in the magnitude of global $[Ca^{2+}]_i$, the extent of maximal ERK1/2 phosphorylation was comparable (Fig.1 and Fig. 6), further supporting our hypothesis that only a proportion of global Ca^{2+} entry by VEGF is associated with ERK1/2 activation in a spatially-restricted manner. Thus although in the case of VEGF the Ca^{2+} response is more prominent, it does not follow that the Na^+ response would also be more pronounced since additional ionic mechanisms can contribute to the global Ca^{2+} rise. Moreover, it is conceivable that in the case of VEGF, generated DAG could be rapidly degraded and/or sequestered, consequently shutting down or confining the Na^+ signal. On the contrary, since OAG was reportedly a poor substrate for the lipases that break down DAG [43] it is expected to have a longer half-life in cells hence magnifying the bulk Na^+ transient measured in or experiments. This is probable since our experiments with the “slow” Ca^{2+} chelator EGTA-AM, indicated that Ca^{2+}-sensitive ERK1/2 activation occurred within 100nm of the source of Ca^{2+} entry. Consequently, the associated Na^+ signal should likewise be spatially restricted. Little is known about Na^+ signalling in ECs, however, such a mechanism has been reported in pancreatic islet β cells where Na^+ influx via plasma membrane VGSCs resulted in significant Na^+ uptake by the mitochondria [44]. Possibly measuring Na^+ signals in single cells could provide better sensitivity. Despite the failure to measure $[Na^+]$ in VEGF-stimulated HUVECs with our experimental setup, our work strongly suggests that Na^+ signals could be also playing a crucial role in endothelial pathophysiology and their significance merits further investigation.

4.5. OAG promotes HUVEC tubular differentiation by activating TRPC3 and NCX

We show here for the first time that OAG application promotes HUVEC tubular differentiation in an *in vitro* surrogate assay for neo-angiogenesis [45]. ERK1/2 activation is crucial for endothelial tubular differentiation [8] and indeed an inhibitor of the ERK1/2 pathway

suppressed OAG-induced tubulogenesis. EC tubule formation was also observed when control cells were plated on ECM in the absence of OAG. This was also significantly suppressed by the ERK1/2 pathway inhibitor (Section 3.9.; Fig. 9). Crucially, both TRPC3 and NCX1 inhibitors and siRNA significantly suppressed OAG-induced HUVEC tubular differentiation, presumably by modulating ERK1/2 activation. Interestingly, both TRPC3 inhibitors and siRNA appear to inhibit HUVEC tubulogenesis more potently than the ERK1/2 pathway inhibitor or reverse-mode NCX inhibitors and siRNA. Although this could be due to different pharmacokinetics (stability and/or cellular uptake) or more efficient TRPC3 knock down, it is plausible that TRPC3 activity could be modulating additional pro-angiogenic signalling pathways. This has been demonstrated in cardiomyocytes where TRPC3 modulated both Ca^{2+} influx via VGCCs and nuclear factor of activated T-cells (NFAT) activation by distinct ionic mechanisms [33].

4.6. Limitations of the study

Our work does not preclude the involvement of other channels of the *Trp* gene family in the EC angiogenic responses observed. Indeed, TRPC1 [46] and TRPC6 [15], [16] activities have also been implicated in angiogenesis. TRPC3 is known to complex with other TRPC isoforms, forming functional non-selective cation channels, including TRPC1 [47] and TRPC6 [48]. Since the composition of native TRPC channels in ECs is unknown, the involvement of other TRPC channels in the macromolecular complex that could potentially reverse the mode of NCX in our experimental setting cannot be excluded. Determining the exact subunit composition of the TRPC3 channel contributing to angiogenesis in HUVECs merits further investigation. However, this is beyond the scope of the present study. Moreover, it is conceivable that other Na^+ influx mechanisms could also become functionally associated with NCX to modulate endothelial signalling, depending on the stimulus/insult. For example, in astrocytes acidification led to Na^+ entry via the $Na^+/HCO3^-$ co-transporter resulting in reversal of NCX [49]. This mechanism could be applicable in tumour angiogenesis where hypoxia results in considerable acidosis.

Recently, Pyr3 at low micromolar concentrations, as those used in the present study, was shown to inhibit the activity of TWIK – related K^+ channels (TREK); [50]. In the endothelium TREK channels are believed to be activated by stretch and participate in the maintenance of vascular tone [51]. Given that our experiments were performed under static conditions, in all probability TREK channels were not involved. However, TREK involvement should be considered, if Pyr3 was used to inhibit *in vivo* angiogenesis.

Interestingly, similar to our previous work with VEGF [11] and thrombin [25], it appears that TRPC3 and reverse-mode NCX inhibitors have an impact on ERK1/2

phosphorylation at baseline. This phenomenon is difficult to reliably quantify since baseline ERK1/2 phosphorylation levels are approximately 15-fold less than the maximal activation observed upon stimulation with VEGF or OAG, as judged by densitometry. Hence its prominence strongly depends on technical factors such as film exposure and identical protein loading between experimental repeats. TRPC3 is known to possess some basal activity *in vitro* in the absence of stimulation [52]. It is probable that this is sufficient to induce some baseline ERK1/2 activation and this could occur via reverse-mode NCX and inhibited by TRPC3 and NCX1 siRNA and inhibitors. Despite the technical difficulties, exploring basal ERK1/2 activity and its associated mechanisms merits further investigation, particularly since ECs are known to be tonically active *in vivo*. Nonetheless, elucidating the mechanism(s) contributing to basal ERK1/2 activation in HUVECs is beyond the scope of the present study.

We also observed baseline inhibition of HUVEC tubulogenesis by TRPC3 inhibitors and siRNA. This is in agreement with studies by others in the HUVEC-derived cell line EA.hy926 [17]. It is well documented that HUVECs can form tubules on extracellular matrices in the absence of growth factors, probably via activation of integrin receptors which in turn could complex with VEGFR2 and modulate its activity [53]. It appears that basal tubulogenesis to some degree also required TRPC3 and reverse-mode NCX activities. However, the upstream activator of ECM-induced tubulogenesis has not been conclusively established and is beyond the scope of this study.

5. Conclusions

To summarise, our results are consistent with the following mechanistic model: VEGFR2 activation by VEGF ligation leads to DAG generation via PLCγ1. Subsequent activation of the DAG-sensitive non-selective cation channel TRPC3 results in Na^+ influx, followed by Ca^{2+} entry by the induction of reverse-mode NCX. This targets PKCα to the plasma membrane, where it becomes fully activated resulting in ERK1/2 phosphorylation and subsequent endothelial tubular differentiation and angiogenesis (Figure 10). Other associated mechanisms such as the membrane potential modulated by VGSCs [10], the Na^+-K^+-ATPase and Na^+ uptake by the mitochondria (omitted here for simplicity) could further refine the angiogenic response.

Collectively, our present work with TRPC3 and our previous studies with VGSC [10] and NCX [11], support the notion that Ca^{2+} entry via reverse-mode NCX and the associated ionic mechanisms play a crucial role in endothelial signalling and neo-angiogenesis *in vitro*. Very little is known about the role of stromal ionic activities in preclinical models of abnormal angiogenesis. Recently, Puro and colleagues elegantly measured the membrane potential and pharmacologically assessed the predominant ionic currents operating in actively

angiogenic vessels of hypoxic mouse retinas *ex vivo* [54]. Intriguingly, the second most prominent current was found to be mediated by reverse-mode NCX, followed by non-selective cation currents, presumably conducted by TRPCs, supporting our *in vitro* findings in HUVEC It is probable that similar ionic mechanisms operate in the highly hypoxic vessels of solid tumours *in* vivo [1], [2]. We envisage that targeting the reverse-mode NCX-TRPC3 signalling complex could be advantageous in conditions characterised by dysregulated angiogenesis.

REFERENCES

1) Potente, M., Gerhardt, H., Carmeliet, P. (2011) Basic and therapeutic aspects of angiogenesis. *Cell*. **146**, 873-87
2) Carmeliet, P., Jain, R. K. (2011) Molecular mechanisms and clinical applications of angiogenesis. *Nature*. **473**, 298-307
3) De Bock, K., Mazzone, M., Carmeliet, P. (2011) Antiangiogenic therapy, hypoxia, and metastasis: risky liaisons, or not? *Nat. Rev. Clin. Oncol*. **8**, 393-404
4) Jayson, G. C., Kerbel, R., Ellis, L. M., Harris, A. L. (2016) Antiangiogenic therapy in oncology: current status and future directions. *Lancet.* **388**, 518-529
5) Simons, M., Gordon, E., Claesson-Welsh, L. (2016) Mechanisms and regulation of endothelial VEGF receptor signalling. *Nat. Rev. Mol. Cell. Biol.* **17**, 611-25.
6) Takahashi, T., Ueno, H., Shibua, M. (1999) VEGF activates protein kinase C-dependent, but Ras-independent Raf-MEK-MAP kinase pathway for DNA synthesis in primary endothelial cells. *Oncogene*. **18**, 2221-30.
7) Breslin, J.W., Pappas, P.J., Cerveira, J.J., Hobson, R.W. 2nd, Durán, W.N. (2003) VEGF increases endothelial permeability by separate signaling pathways involving ERK-1/2 and nitric oxide. *Am. J. Physiol. Heart Circ. Physiol*. **284**, H92-H100
8) Mavria, G., Vercoulen, Y., Yeo, M., Paterson, H., Karasarides, M., Marais, R., Bird, D., Marshall, C.J. (2006) ERK-MAPK signaling opposes Rho-kinase to promote endothelial cell survival and sprouting during angiogenesis. *Cancer Cell*. **9**, 33-44
9) Chamorro-Jorganes, A., Lee, M.Y., Araldi, E., Landskroner-Eiger, S., Fernández-Fuertes, M., Sahraei, M., Quiles Del Rey, M., van Solingen, C., Yu, J., Fernández-Hernando, C., Sessa, W.C., Suárez, Y. (2016) VEGF-Induced Expression of miR-17-92 Cluster in Endothelial Cells Is Mediated by ERK/ELK1 Activation and Regulates Angiogenesis. *Circ. Res*. **118**, 38-47
10) Andrikopoulos, P., Fraser, S.P., Patterson, L., Ahmad, Z., Burcu, H., Ottaviani, D., Diss, J.K., Box, C., Eccles, S.A., Djamgoz, M.B. (2011) Angiogenic functions of voltage-gated Na+ Channels in human endothelial cells: modulation of vascular endothelial growth factor (VEGF) signaling. *J. Biol. Chem*. **286**, 16846-60
11) Andrikopoulos, P., Baba, A., Matsuda, T., Djamgoz, M.B., Yaqoob, M.M., Eccles, S.A. (2011) Ca2+ influx through reverse mode Na+/Ca2+ exchange is critical for vascular endothelial growth factor-mediated extracellular signal-regulated kinase (ERK) 1/2 activation and angiogenic functions of human endothelial cells. *J. Biol. Chem*. **286**, 37919-31

12) Dawson, N.S., Zawieja, D.C., Wu, M.H., Granger, H.J. (2006) Signaling pathways mediating VEGF165-induced calcium transients and membrane depolarization in human endothelial cells. *FASEB J*. **20**, 991-3
13) Fiorio Pla, A., Munaron, L. (2014) Functional properties of ion channels and transporters in tumour vascularization. *Philos. Trans. R. Soc. Lond. B Biol. Sci.* **369**, (1638)
14) Cheng, H.W., James, A.F., Foster, R.R., Hancox, J.C., Bates, D.O. (2006) VEGF activates receptor-operated cation channels in human microvascular endothelial cells. *Arterioscler. Thromb. Vasc. Biol.* **26**, 1768-1776
15) Hamdollah Zadeh, M.A., Glass, C.A., Magnussen, A., Hancox, J.C., Bates, D.O. (2008) VEGF-mediated elevated intracellular calcium and angiogenesis in human microvascular endothelial cells in vitro are inhibited by dominant negative TRPC6. *Microcirculation* **15**, 605-614
16) Ge, R., Tai, Y., Sun, Y., Zhou, K., Yang, S., Cheng, T., Zou, Q., Shen, F., Wang, Y. (2009) Critical role of TRPC6 channels in VEGF-mediated angiogenesis. *Cancer Lett*. **283**, 43-51
17) Antigny, F., Girardin, N., Frieden, M. (2012) Transient receptor potential canonical channels are required for in vitro endothelial tube formation. *J. Biol. Chem*. **287**, 5917-27
18) Li, J., Cubbon, R.M., Wilson, L.A., Amer, M.S., McKeown, L., Hou, B., Majeed, Y., Tumova, S., Seymour, V.A., Taylor, H., Stacey, M., O'Regan, D., Foster, R., Porter, K.E., Kearney, M.T., Beech, D.J. (2011) Orai1 and CRAC channel dependence of VEGF-activated Ca2+ entry and endothelial tube formation. Circ Res. **108**, 1190-8
19) Khananshvili, D. (2016) The SLC8 gene family of sodium-calcium exchangers (NCX) - structure, function, and regulation in health and disease. Mol. Aspects Med. 34, 220-35
20) Imahashi, K., Pott, C., Goldhaber, J.I., Steenbergen, C., Philipson, K.D., Murphy, E. (2005) Cardiac-specific ablation of the Na+-Ca2+ exchanger confers protection against ischemia/reperfusion injury. *Circ. Res.* **97**, 916-921
21) Li, L.., van Breemen, C. (1995) Na+-Ca2+ exchange in intact endothelium of rabbit cardiac valve. *Circ. Res*. **76**, 396–404
22) Sedova, M., Blatter, L.A. (1999) Dynamic regulation of [Ca2+]i by plasma membrane Ca2+-ATPase and Na+/Ca2+ exchange during capacitative Ca2+ entry in bovine vascular endothelial cells. *Cell Calcium* **25**, 333–343
23) Szewczyk, M.M., Davis, K.A., Samson, S.E., Simpson, F., Rangachari, P.K., Grover, A.K. (2007) Ca2+-pumps and Na2+-Ca2+-exchangers in coronary artery endothelium versus smooth muscle. *J. Cell. Mol. Med*. **11**, 129–138
24) Rosker, C., Graziani, A., Lukas, M., Eder, P., Zhu, M.X., Romanin, C., Groschner, K. (2004)Ca(2+) signaling by TRPC3 involves Na(+) entry and local coupling to the Na(+)/Ca(2+) exchanger. *J. Biol. Chem*. **279**, 13696-704
25) Andrikopoulos, P., Kieswich, J., Harwood, S.M., Baba, A., Matsuda, T., Barbeau, O., Jones, K., Eccles, S.A., Yaqoob M.M. (2015) Endothelial Angiogenesis and Barrier Function in Response to Thrombin Require Ca2+ Influx through the Na+/Ca2+ Exchanger. *J. Biol. Chem*. **290**, 18412-28
26) Kiyonaka, S., Kato, K., Nishida, M., Mio, K., Numaga, T., Sawaguchi, Y., Yoshida, T., Wakamori, M., Mori, E., Numata, T., Ishii, M., Takemoto, H., Ojida, A., Watanabe, K., Uemura, A., Kurose, H., Morii, T., Kobayashi, T., Sato, Y., Sato, C., Hamachi, I.,

Mori, Y. (2009) Selective and direct inhibition of TRPC3 channels underlies biological activities of a pyrazole compound. *Proc Natl Acad Sci U S A*. **106**, 5400-5
27) Schleifer, H., Doleschal, B., Lichtenegger, M., Oppenrieder, R., Derler, I., Frischauf, I., Glasnov, T.N., Kappe, C.O., Romanin, C., Groschner, K. (2012) Novel pyrazole compounds for pharmacological discrimination between receptor-operated and store-operated Ca(2+) entry pathways. *Br. J. Pharmacol*. **167**, 1712-1722
28) Wong, C., Jin, Z.G. (2005) Protein kinase C-dependent protein kinase D activation modulates ERK signal pathway and endothelial cell proliferation by vascular endothelial growth factor. *J. Biol. Chem*. **280**, 33262-9
29) Xia, P., Aiello, L.P., Ishii, H., Jiang, Z.Y., Park, D.J., Robinson, G.S., Takagi, H., Newsome, W.P., Jirousek, M.R., King, G.L.(1996) Characterization of vascular endothelial growth factor's effect on the activation of protein kinase C, its isoforms, and endothelial cell growth. *J. Clin. Invest*. **98**, 2018-26.
30) Hofmann, T., Obukhov, A.G., Schaefer, M., Harteneck, C., Gudermann, T., Schultz, G. (1999) Direct activation of human TRPC6 and TRPC3 channels by diacylglycerol. *Nature*. **397**, 259-63.
31) Trebak, M., St J Bird, G., McKay, R.R., Birnbaumer, L., Putney, J.W. Jr. Signaling mechanism for receptor-activated canonical transient receptor potential 3 (TRPC3) channels. *J. Biol. Chem*. **278**, 16244-52.
32) Parekh, A.B. (2008) Ca2+ microdomains near plasma membrane Ca2+ channels: impact on cell function. *J. Physiol*. **586**, 3043–3054
33) Poteser, M., Schleifer, H., Lichtenegger, M., Schernthaner, M., Stockner, T., Kappe, C.O., Glasnov, T.N., Romanin, C., Groschner, K. (2011) PKC-dependent coupling of calcium permeation through transient receptor potential canonical 3 (TRPC3) to calcineurin signaling in HL-1 myocytes. *Proc. Natl. Acad. Sci. U .S. A*. **108**, 10556-61
34) Groschner, K., Hingel, S., Lintschinger, B., Balzer, M., Romanin, C., Zhu, X., Schreibmayer, W. (1998) Trp proteins form store-operated cation channels in human vascular endothelial cells. *FEBS Lett*. **437**, 101-6.
35) Smedlund, K., Tano, J-Y., Vazquez, G. (2010) The constitutive function of native TRPC3 channels modulates vascular cell adhesion molecule-1 expression in coronary endothelial cells through nuclear factor kappaB signaling. *Circ. Res.* **106**, 1479–1488
36) Smedlund, K.B., Birnbaumer, L., Vazquez, G. (2015) Increased size and cellularity of advanced atherosclerotic lesions in mice with endothelial overexpression of the human TRPC3 channel. *Proc. Natl. Acad. Sci. U .S. A.* **112**, 2201-6
37) Doleschal, B., Primessnig, U., Wölkart, G., Wolf, S., Schernthaner, M., Lichtenegger, M., Glasnov, T.N., Kappe, C.O., Mayer, B., Antoons, G., Heinzel, F., Poteser, M., Groschner, K. (2015) TRPC3 contributes to regulation of cardiac contractility and arrhythmogenesis by dynamic interaction with NCX1. *Cardiovasc. Res*. **106**, 163-73.
38) Poburko, D., Liao, C. H., Lemos, V. S., Lin, E., Maruyama, Y., Cole, W. C., van Breemen, C. (2007) Transient receptor potential channel 6-mediated, localized cytosolic [Na+] transients drive Na+/Ca2+ exchanger-mediated Ca2+ entry in purinergically stimulated aorta smooth muscle cells. *Circ. Res*. **101**, 1030–1038
39) Harper, M.T., Londoño, J.E., Quick, K., Londoño, J.C., Flockerzi, V., Philipp, S.E., Birnbaumer, L., Freichel, M., Poole, A.W. (2013)Transient receptor potential channels function as a coincidence signal detector mediating phosphatidylserine exposure. *Sci Signal*. **6**(281):ra50.

40) Abdullaev, I.F., Bisaillon, J.M., Potier, M., Gonzalez, J.C., Motiani, R.K., Trebak, M. (2008) Stim1 and Orai1 mediate CRAC currents and store-operated calcium entry important for endothelial cell proliferation. *Circ. Res*. **103**, 1289-99
41) Kamouchi, M., Philipp, S., Flockerzi, V., Wissenbach, U., Mamin, A., Raeymaekers, L., Eggermont, J., Droogmans, G., Nilius, B. (1999) Properties of heterologously expressed hTRP3 channels in bovine pulmonary artery endothelial cells. J. Physiol. 518, 345-358
42) Orci,L., Ravazzola, M., Le Coadic, M., Shen, W.W., Demaurex, N., Cosson, P. (2009) STIM1-induced precortical and cortical subdomains of the endoplasmic reticulum. *Proc. Natl. Acad. Sci. U .S. A.* **106**, 19358–19362.
43) Florin-Christensen, J., Florin-Christensen, M., Delfino, J.M., Rasmussen, H. (1993) New patterns of diacylglycerol metabolism in intact cells. *Biochem J*. **289**, 783–788.
44) Nita, I.I., Hershfinkel, M., Lewis, E.C., Sekler, I. (2015) A crosstalk between Na^+ channels, Na^+/K^+ pump and mitochondrial Na^+ transporters controls glucose-dependent cytosolic and mitochondrial Na^+ signals. *Cell Calcium*. **57**, 69-75
45) Eccles, S.A., Court, W., Patterson, L. (2016) In Vitro Assays for Endothelial Cell Functions Required for Angiogenesis: Proliferation, Motility, Tubular Differentiation, and Matrix Proteolysis. *Methods Mol. Biol.* **1430**, 121-47
46) Yu, P.C., Gu, S.Y., Bu, J.W., Du, J.L. (2010) TRPC1 is essential for in vivo angiogenesis in zebrafish. *Circ Res*. **106**, 1221-32
47) Zagranichnaya, T.K., Wu, X., Villereal, M.L. (2005) Endogenous TRPC1, TRPC3, and TRPC7 proteins combine to form native store-operated channels in HEK-293 cells. *J. Biol. Chem*. **280**, 29559-69
48) Hofmann, T., Schaefer, M., Schultz, G., Gudermann, T. (2002) Subunit composition of mammalian transient receptor potential channels in living cells. *Proc. Natl. Acad. Sci. U. S. A.* **99**, 7461-6.
49) Turovsky, E., Theparambil, S.M., Kasymov, V., Deitmer, J.W., Del Arroyo, A.G., Ackland, G.L., Corneveaux, J.J., Allen, A.N., Huentelman, M.J., Kasparov, S., Marina, N., Gourine, A.V. (2016) Mechanisms of CO2/H+ Sensitivity of Astrocytes. *J. Neurosci.* **36**, 10750-10758.
50) Kim, H.J., Woo, J., Nam, Y., Nam, J.H., Kim, W.K. (2016) Differential modulation of TWIK-related K+ channel (TREK) and TWIK-related acid-sensitive K+ channel 2 (TASK2) activity by pyrazole compounds. *Eur. J. Pharmacol*. **791**, 686-695.
51) Goonetilleke, L., Quayle, J. (2012) TREK-1 K(+) channels in the cardiovascular system: their significance and potential as a therapeutic target. *Cardiovasc. Ther*. *30*: e23-9
52) Smedlund, K., Bah, M., Vazquez, G. (2012) On the Role of Endothelial TRPC3 Channels in Endothelial Dysfunction and Cardiovascular Disease. *Cardiovasc. Hematol. Agents Med. Chem*. **10**, 265–274.
53) Mahabeleshwar, G.H., Chen, J., Feng, W., Somanath, P.R., Razorenova, O.V., Byzova, T.V. (2008) Integrin affinity modulation in angiogenesis. *Cell Cycle*. **7**, 335-47.
54) Puro, D.G., Kohmoto, R., Fujita, Y., Gardner, T.W., Padovani-Claudio, D.A. (2016) Bioelectric impact of pathological angiogenesis on vascular function. *Proc. Natl. Acad. Sci. U. S. A.* **113**, 9934-9.

ACKNOWLEDGMENTS

This work was directly funded by the Barts and the London National Institute of Health Research (NIHR) Cardiovascular Biomedical Research Unit. Support to PA and MMY by the Barts Health "Diabetic Kidney Disease Centre," supported and funded by the Barts and the London Charity is gratefully acknowledged. SAE receives funding from The Institute of Cancer Research and Cancer Research United Kingdom Grant C309/A8274. The authors wish to thank Sam Ranasinghe (University College London) for assistance with the FLIPR – Tetra assays.

CONFLICT OF INTEREST

None

FIGURE LEGENDS

Figure 1. TRPC3 activity is required for VEGF-induced ERK1/2 phosphorylation. A, Serum-starved HUVECs were preincubated with the specific TRPC3 inhibitor Pyr3 (10μM) or vehicle for 30min prior to addition of VEGF (50ng/ml) for the indicated times. ERK1/2 activation was probed by Western blot. Membranes were subsequently stripped and re-probed with a total-ERK1/2 antibody to ensure equal protein loading. B, The effect of Pyr3 on PLCγ1 and ERK1/2 activation was also assessed over a range of doses in HUVECs stimulated for 10min with VEGF (50ng/ml). C, Normalized optical densities of the phospho-ERK1/2 and phospho-PLCγ1 bands against the corresponding total-ERK1/2 loading controls. The value of the unstimulated control level (bar C) was arbitrarily set to 1 and all other values were calculated as fold changes relative to bar C. *Bars* represent the means ± S.E. from n = 3 experiments. *, $p < 0.05$ *versus* the VEGF-stimulated control. A second specific TRPC3 inhibitor Pyr10 (10μM) also attenuated VEGF-induced ERK1/2 activation in a time-dependent manner (D). The effect of Pyr10 on PLCγ1 and ERK1/2 phosphorylation was also investigated over a range of doses (*E*) and quantified (F) as described in (C). Data are expressed as the means ± S.E. from n = 3 experiments. *, $p < 0.05$ *versus* the VEGF-stimulated control. G, HUVECs were transfected with TRPC3-targeting or control non-targeting siRNA duplexes. After 48h, cells were serum-starved and challenged with VEGF (50ng/ml) for 10min. ERK1/2 phosphorylation and TRPC3 protein levels were determined as described in (A). Relative optical densities of phospho-ERK1/2 (H) and TRPC3 (I) were assessed as in (C). Data are shown as the means ± S.E. from n = 3 experiments *, $p < 0.05$ *versus* the VEGF-stimulated control. For (*I*) *, $p < 0.05$ *versus* the non-targeting siRNA-treated control.

Figure 2. TRPC3 activity is required for VEGF-induced PKCμ/PKD phosphorylation and PKCα translocation to the membrane fraction. A**,** Serum-starved HUVECs were challenged with VEGF in the presence of the TRPC3 inhibitor Pyr3 (3μM), the CRAC inhibitor Pyr6 (10μM) or vehicle. Phospho-PKCμ/PKD, phospho-ERK1/2 or total ERK1/2 levels were determined by Western blot as described in Fig. 1A. Densitometric values of fold changes of normalized phospho-PKCμ/PKD (B) or phospho-ERK1/2 (*C*) ratios were assessed as described in Fig. 1*C*. Values from n=3 independent experiments are shown as the means ± S.E for both *(*B) and (C). *, $p < 0.05$ VEGF in the presence of Pyr3 values *versus* the VEGF-stimulated control. $^{\#}$, $p < 0.05$ VEGF in the presence of Pyr6 values *versus* the VEGF – stimulated control. D, Serum-starved HUVECs were stimulated with ionomycin

(1μM) for 5min in the presence of Pyr3 (10μM), Pyr10 (10μM), Pyr6 (10μM) or vehicle as indicated. ERK1/2 activation was evaluated by Western blot as in Fig. 1A). E, Cytosolic and membrane fractions from control (C) or VEGF-stimulated HUVECs in the presence or absence of the TRPC3 inhibitors Pyr3 (3μM) and Pyr10 (10μM), or vehicle were separated by ultracentrifugation. PKCα translocation to the crude membrane fraction and the presence of the plasma membrane marker Na^+-K^+-ATPase or the cytosolic marker GAPDH, were assessed by Western blot. F, Densitometric analysis of PKCα levels in the membrane fraction, normalized by optical density of Na^+-K^+-ATPase in each corresponding sample are shown. Data are presented as the means ± S.E. and were from *n* = 3 experiments *, $p < 0.05$ *versus* the VEGF-stimulated control. G, HUVECs were stimulated with the PKC activator PMA (1μM) for 10min in the presence of Pyr3 (10μM) or Pyr10 (10μM) as indicated, *n* = 3 independent experiments.

Figure 3. TRPC3 inhibitors attenuate VEGF-induced Ca^{2+} transients. (A) Representative Fluo-4NW Ca^{2+}-sensitive fluorescence of HUVECs stimulated with VEGF (50ng/ml) over time in the presence of TRPC3 inhibitors or vehicle are shown. VEGF was added at time 0 and after a mix step fluorescence was measured every 2sec. Blue traces represent unstimulated control, red traces VEGF-stimulated cells, green traces cells preincubated with Pyr3 (3μM) prior to VEGF stimulation and purple traces cells preincubated with Pyr10 (10μM) prior to VEGF stimulation. (B), Area under the curve of the Ca^{2+} transients shown in (*A*) calculated as fold changes in relation to the unstimulated control (arbitrarily set to 1). Bars represent means ± S.E. (*n* = 3 in triplicate). *, $p < 0.05$ *versus* VEGF-stimulated control.

Figure 4. TRPC3 activity is required for VEGF-induced HUVEC tubular differentiation on ECM components. (A) HUVECs in Opti-MEM-I® medium containing 0.2% v/v FCS in the presence or absence of VEGF (50ng/ml) were seeded in 24-well plates coated with growth factor-reduced Matrigel™. Where appropriate the indicated concentrations of the specific TRPC3 inhibitors Pyr3 and Pyr10 or vehicle were also included, as appropriate. Images from 5 random fields of view were obtained after 16h and representative images at 10x magnification are shown for each experimental treatment. (B) Tubule length was quantified from the images taken in (A). Mean tubule length of the unstimulated control (C) was set to 1. Bars represent means ± S.E. (n = 3 in duplicate). *, $p < 0.05$ versus the corresponding control. (C) images of HUVECs transfected with control non-targeting or TRPC3-targeting siRNA with or without VEGF and seeded on Matrigel™ as in (*A*) for 4h. (D), quantification of tubule length from *n*=3 in duplicate experiments from (*C*) was carried out as described in (B)

Figure 5. ERK1/2 activation by the diacylglycerol cell-permeable analogue 1-Oleoyl-2-acetyl-sn-glycerol (OAG) requires extracellular Ca^{2+} and PKC activity. A, Serum-starved HUVECs were loaded with the "fast" Ca^{2+} chelator BAPTA-AM or with the "slow" Ca^{2+} chelator EGTA-AM for a further 20min prior to stimulation with the TRPC3 activator OAG (100μM) for 5min. ERK1/2 activation was assessed with Western blot as in Fig. 1A. B, HUVECs were serum-starved for 45min and then switched to a Ca^{2+}-free buffer for a further 15min prior to challenge with OAG (100μM) or vehicle for 5min. ERK1/2 phosphorylation was assessed by Western blot as before. C, HUVECs incubated in complete physiological buffer or in a medium where Ca^{2+} has been omitted were challenged with thapsigargin (TG) for 2min. Subsequently, where appropriate, cells were stimulated with OAG (100μM) for a further 5min. ERK1/2 phosphorylation was probed as in Fig. 1*A*. D, Serum-starved HUVECs were incubated with the indicated concentrations of the broad spectrum PKC inhibitor

Gö6983, or vehicle for 30min. Subsequently, OAG (100μM) was added to the bath and ERK1/2 activation was assessed as in Fig. 1*A*. For all the experiments *n* = 3

Figure 6. **TRPC3 activity was required for OAG-induced ERK1/2 activation and Ca^{2+} transients**. A, HUVECs were preincubated with the indicated concentrations of the specific TRPC3 inhibitor Pyr3 or vehicle, for 30min, prior to stimulation with the TRPC3 activator OAG (100μM) for further 5min and ERK1/2 phosphorylation was determined as in Fig. 1A. B, The optical densities of the phospho-ERK1/2 bands were normalised with the corresponding total-ERK1/2 loading controls and were shown as described in Fig. 1C. Data are shown as the means ± S.E. from *n* = 3 experiments. *, $p < 0.05$ *versus* the OAG-stimulated control. C, Cells were transfected with control non-targeting siRNA or TRPC3-targeting siRNA (100nM for 48h), serum-starved and subsequently stimulated with OAG (100μM) for 5min. ERK1/2 activation (D) and TRPC3 expression (E) were quantified by densitometry as described in Fig. 1C. Values are expressed as means ± S.E. from *n* = 3 experiments *, $p < 0.05$ *versus* the OAG-stimulated control for both (D) and (E). *F*, HUVECs were preincubated with the VGCC inhibitor nifedipine (1μM) prior to stimulation with OAG (100μM) and ERK1/2 phosphorylation was determined by Western blot as described in Fig. 1A.

Figure 7. Ca^{2+} influx via reverse-mode NCX is required for OAG-induced ERK1/2 phosphorylation. A, HUVECs were preincubated with the reverse-mode NCX inhibitor SN-6 (10μM) or vehicle for 30min and subsequently stimulated with the TRPC3 activator OAG (100μM) as indicated. ERK1/2 activation was assessed as in Fig. 1A. B, HUVECs were incubated with the indicated concentrations of a second reverse-mode NCX inhibitor, SEA0400, for 30min prior to stimulation with OAG (100μM) for 5min. ERK1/2 activation was assessed by Western blot as before. *C*, Densitometric analysis of ERK1/2 phosphorylation of the experiments in B, was as described in Fig. 1C. Values are means ± S.E. from *n* = 3 experiments *, $p < 0.05$ *versus* the OAG-stimulated control. D, HUVECs were transfected with control non-targeting siRNA, or NCX1-targeting siRNA and after 48h were serum-starved and challenged with OAG (100μM) for 5min. ERK1/2 activation was determined by Western blot. E, ERK1/2 activation in D was quantified by densitometry as in Fig. 1C. Values are expressed as means ± S.E. (*n* = 3 in triplicate). *, $p < 0.05$ *versus* control siRNA-treated OAG-stimulated control. F, NCX1 protein levels in control- or NCX1-siRNA treated cells was determined by immunoprecipitation and subsequent Western blots of cell lysates from parallel transfections to those in D. Equal protein in each of the samples for immunoprecipitation was ensured by probing for β-actin in the input. G, Normalized optical densities of the NCX1 bands against the corresponding β-actin input levels of the siRNA transfections in F. Bars represent the means ± S.E. from *n* = 3 experiments. *, $p < 0.05$ versus the control siRNA sample. H, HUVECs were preincubated with the reverse-mode NCX inhibitors SEA0400 (1μM) and SN-6 (10μM), the TRPC3 inhibitors Pyr3 (3μM) and Pyr10 (10μM) or vehicle prior to stimulation with OAG (100μM) as indicated. Changes in $[Ca^{2+}]_i$ were determined by monitoring the emitted fluorescence over time of samples loaded with the Ca^{2+}-indicator Fluo-4NW as described in the Methods section in a FLIPR – TETRA instrument. Blue traces represent unstimulated cells, red traces OAG-stimulated cells, green traces cells preincubated with SEA0400, purple traces cells preincubated with SN-6, light blue traces cells preincubated with Pyr3 and orange traces cell preincubated with Pyr10 prior to OAG stimulation. Traces from a representative experiment are shown. I, Area under the curve of the experiments described in H were calculated as described in the Methods

section. Data are presented as means ± S.E. (n = 3 in triplicate). *, p < 0.05 versus OAG-stimulated control.

Figure 8. OAG-induced Na^+ influx requires TRPC3 activity but is independent of reverse-mode NCX. A, HUVECs were loaded with the Na^+ fluorescent probe Asante NATRIUM Green-2 (ANG-2) in complete physiological medium for 1h. After a 15min preincubation with the reverse-mode NCX inhibitors SEA0400 (1μM), SN-6 (10μM), Pyr3 (3μM) or Pyr10 (10μM) cells were stimulated with the TRPC3 activator OAG (100μM) as indicated and fluorescence was monitored every 2sec in the FLIPR-TETRA instrument. Traces from a representative experiment are shown. B, The area under the curve of the Na^+ transients in A was calculated as described in the Methods section. Values are expressed as means ± S.E. (*n* = 3 in triplicate). *, p < 0.05 versus the unstimulated control. C, HUVECs were challenged with 100μM ouabain for 1min prior to the addition of OAG (100μM) for 2min and ERK1/2 activation was determined by Western blot as described in Figure 1. The indicated samples were incubated with SN-6 (10μM) for 30min prior to OAG addition. D, Densitometric analysis of ERK1/2 activation from the experiments in C was performed as in Fig. 1C. Data are shown as means ± S.E. (*n* = 3). *, p < 0.05 *versus* the OAG-stimulated control. E, Serum-starved HUVECs were pretreated with ouabain prior to stimulation with OAG as described in C. The indicated samples were pre-incubated with the TRPC3 specific inhibitor Pyr3 (3μM) for 30min prior to ouabain addition. ERK1/2 activation was assessed by Western blot.

Figure 9. Increased HUVEC tubular differentiation in response to the DAG analogue OAG required TRPC3, NCX and ERK1/2 pathways activities. (A) HUVECs in Opti-MEM-I® medium containing 0.2% v/v FCS in the presence or absence of the TRPC3 activator OAG (100μM) were seeded in 24-well plates coated with growth factor-reduced Matrigel™. Where appropriate the indicated concentrations of the TRPC3 inhibitor Pyr3, the reverse-mode NCX inhibitor SEA0400, the ERK1/2 pathway inhibitor PD98050 (PD) or vehicle were also added as appropriate. After 4h, images from 5 random fields of view were obtained and representative images at 10x magnification are shown for each experimental treatment. (B) Quantification of tubule length from n=3 in duplicate experimental conditions as described in (A) were analysed as in Fig. 4B. (C) Representative images of tubule formation from HUVECs transfected with non-targeting (control), TRPC3 targeting (TRPC3) or NCX1 targeting (NCX1) siRNA duplexes for 48h and subsequently seeded on Matrigel™ in the presence or absence of OAG as indicated for 4h are shown. (D) Quantification of HUVEC cord length for the experimental conditions in (C) was carried our as described above (*n*=3 in duplicate).

Figure10. TRPC3 and NCX1 activities have an additive effect on VEGF – or OAG – induced ERK1/2 phosphorylation. A, HUVECs were preincubated with Pyr3 (3μM), SN-6 (5μM), or both for 30min prior to stimulation with VEGF (50ng/ml) for 10min as indicated. ERK1/2 activation was assessed by western blot. B, Normalizes optical densities of the phospho-ERK1/2 bands from the experiments described in A. The value of the unstimulated control was arbitrarily set to 1. Bars represent the means ± S.E. from *n* = 3 experiments. *, *p* < 0.05 *versus* the single inhibitor treatment samples. The effect of combining treatment with the inhibitors Pyr3 and SN-6 was also assessed in OAG-stimulated HUVECs (C) and quantified (D) as in B. Data are expressed as the means ± S.E. from *n* = 3 experiments. *, *p* < 0.05 *versus* the single inhibitor treatment samples. E, HUVECs were transfected with TRPC3 – targeting, NCX1 – targeting, control non-targeting siRNA duplexes, or their

combination, as indicated. After 48h, cells were serum-starved and challenged with VEGF (50ng/ml) for 10min. ERK1/2 phosphorylation and TRPC3 protein levels were determined as described in Figure 1A. Relative optical densities of phospho-ERK1/2 (F) for each condition were assessed as in (B). Data are shown as the means ± S.E. from n = 3 experiments *, $p < 0.05$ *versus* the HUVEC samples transfected with only TRPC3 or NCX1 siRNA duplexes. G, NCX1 protein levels in control-, TRPC3- or NCX1-siRNA treated cells was determined by immunoprecipitation and subsequent Western blots of cell lysates from parallel transfections to those in E.

Figure 11. Proposed mechanistic model. Numbers in parenthesis indicate proposed sequence of signalling events. (1) Ligation of VEGF to its major endothelial receptor VEGFR2 results in (2) PLCγ1 activation and generation of (3) diacylglycerol (DAG) and (3) inositol 1,4,5-triphosphate (IP_3). Subsequently, (4) DAG complexes with and activates the DAG-sensitive non-selective cation channel TRPC3 leading to (5) Na^+ influx followed by induction of (6) reverse-mode NCX and Ca^{2+} entry from the extracellular milieu. Increased [Ca^{2+}] in the vicinity of the plasma membrane (7) targets PKCα to the membrane fraction where it complexes with DAG and becomes fully activated resulting in (8) ERK1/2 pathway activation and (9) downstream HUVEC tubular differentiation and angiogenesis. The effects of DAG can be also emulated by the application of the cell-permeable DAG analogue 1-Oleoyl-2-acetyl-sn-glycerol (OAG). Concurrently, Ca^{2+} release from the internal stores via IP_3 receptors (IP_3R) and the membrane potential (V_m) could further shape the NCX mode of action and/or activation and consequently the endothelial angiogenic response. Other associated mechanisms such as modulation of intracellular Na^+ by the Na^+-K^+-ATPase or the mitochondria and/or modulation of intracellular Ca^{2+} by uptake by the sarcoendoplasmc reticulum Ca^{2+} ATPase (SERCA) or extrusion by the plasma membrane Ca^{2+} ATPase (PMCA) could further refine the amplitude of ERK1/2 phosphorylation

FIGURES

Figure 1

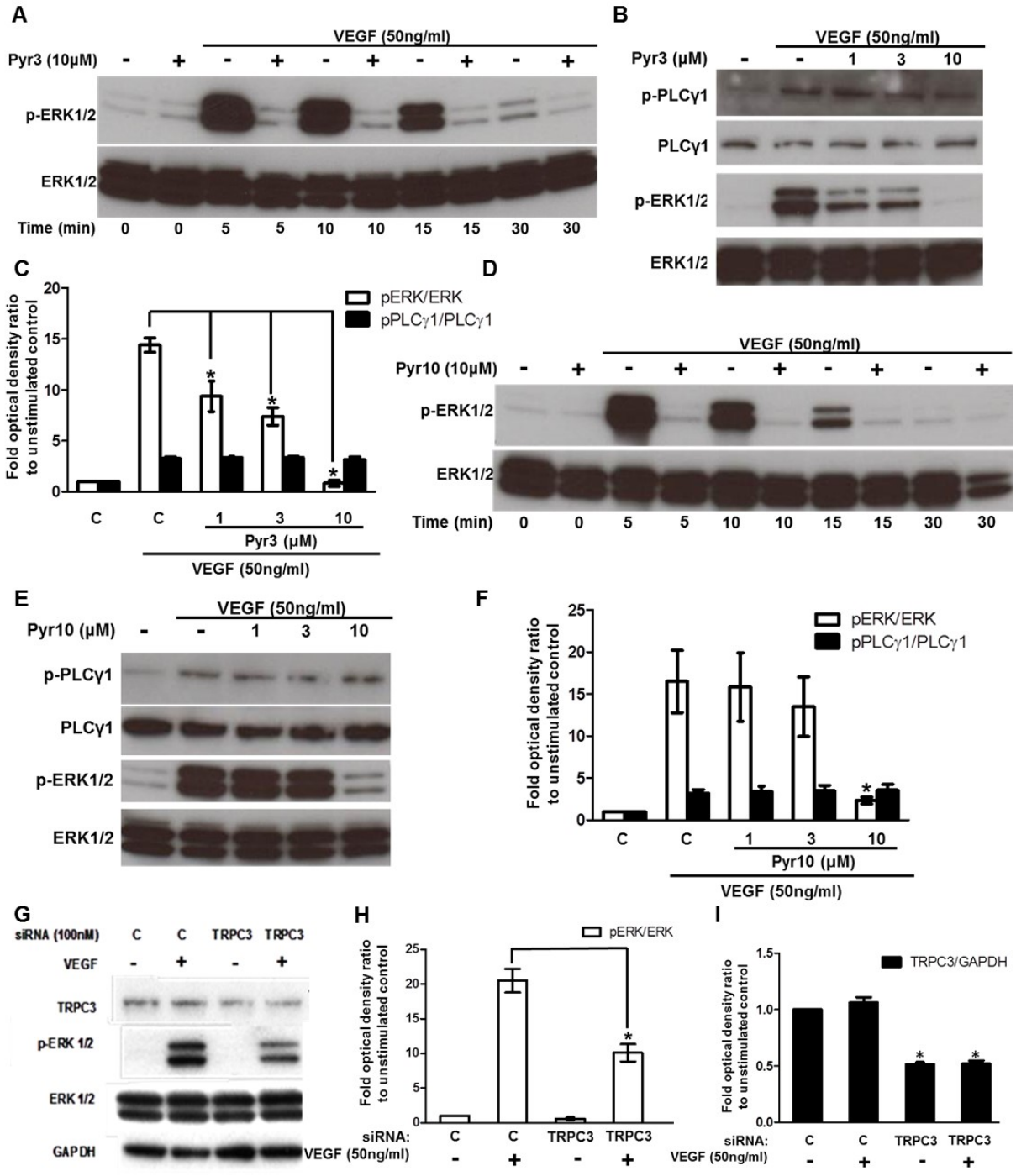

Figure 2

Figure 2

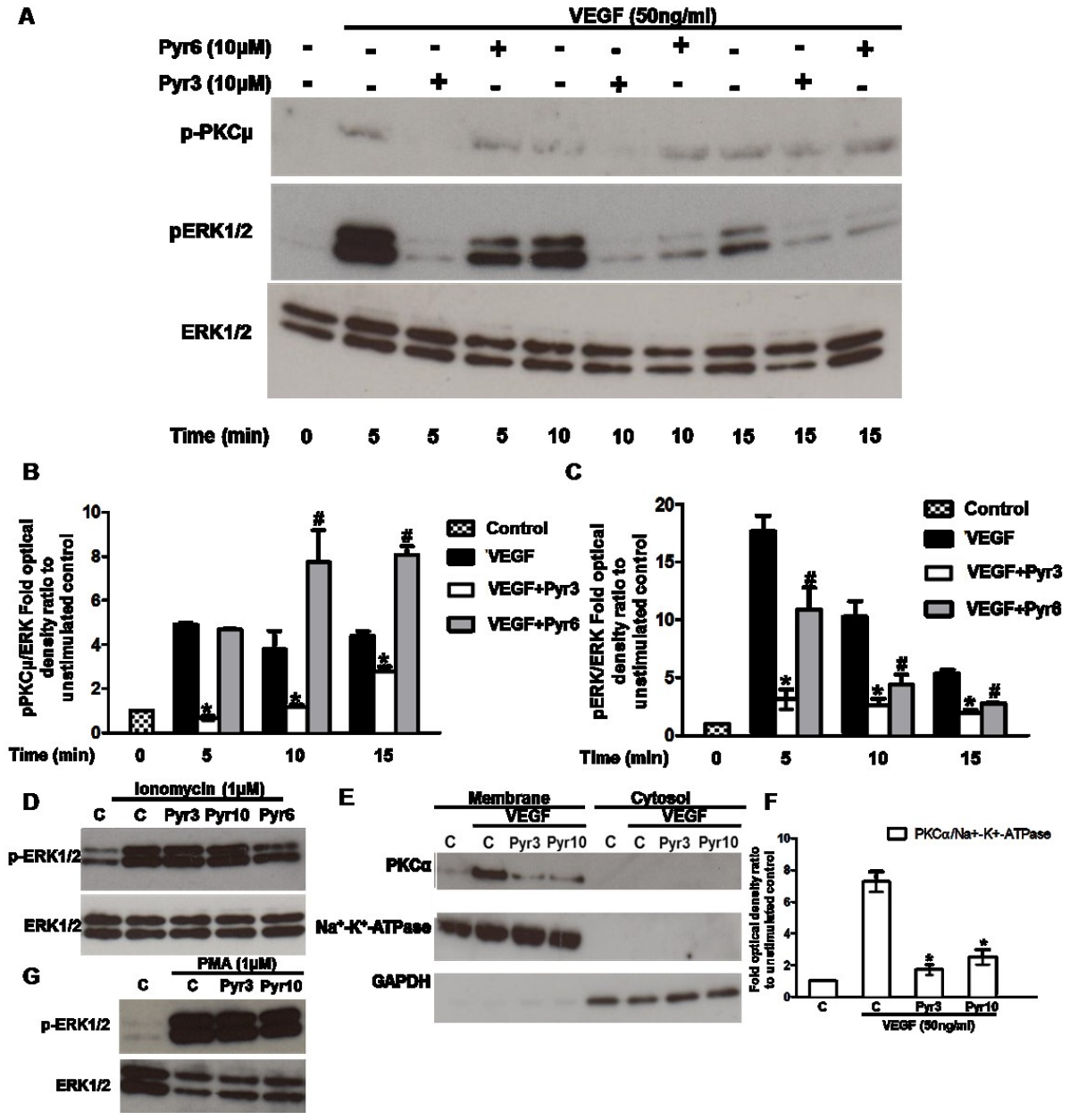

Figure 3

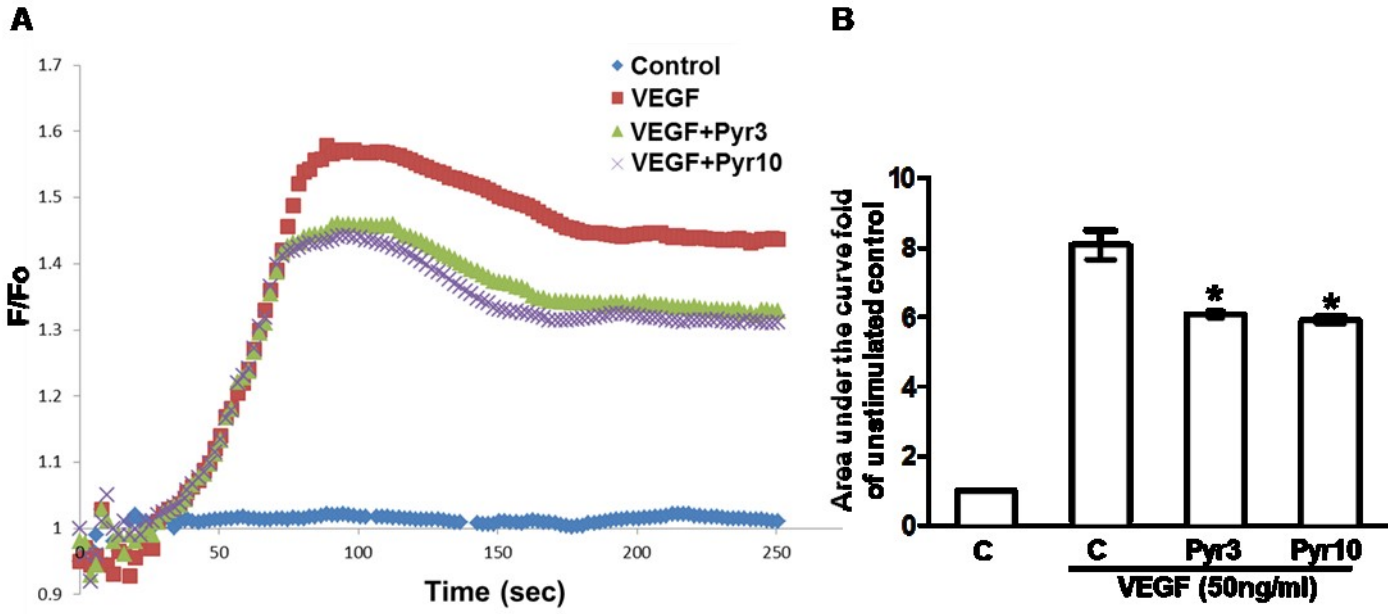
A
B
Control
VEGF
VEGF+Pyr3
VEGF+Pyr10
F/Fo
Time (sec)
Area under the curve fold of unstimulated control
C
C
Pyr3
Pyr10
VEGF (50ng/ml)
*
*

Figure 4

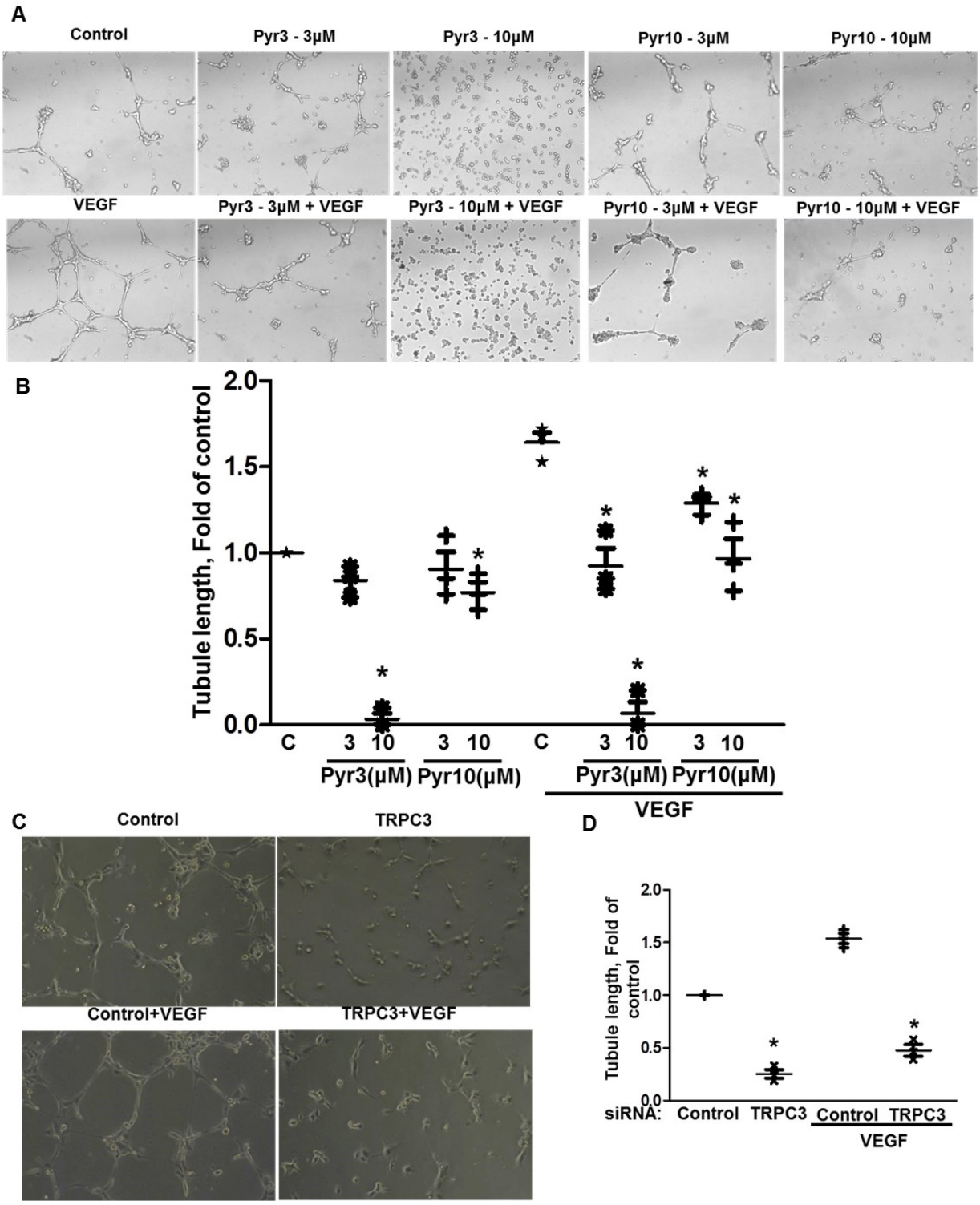
A
Control
Pyr3 - 3μM
Pyr3 - 10μM
Pyr10 - 3μM
Pyr10 - 10μM
VEGF
Pyr3 - 3μM + VEGF
Pyr3 - 10μM + VEGF
Pyr10 - 3μM + VEGF
Pyr10 - 10μM + VEGF
B
Tubule length, Fold of control
2.0
1.5
1.0
0.5
0.0
C
3
10
3
10
C
3
10
3
10
Pyr3(μM)
Pyr10(μM)
Pyr3(μM)
Pyr10(μM)
VEGF
C
Control
TRPC3
Control+VEGF
TRPC3+VEGF
D
Tubule length, Fold of control
2.0
1.5
1.0
0.5
0.0
siRNA:
Control
TRPC3
Control
TRPC3
VEGF

Figure 5

Figure 5

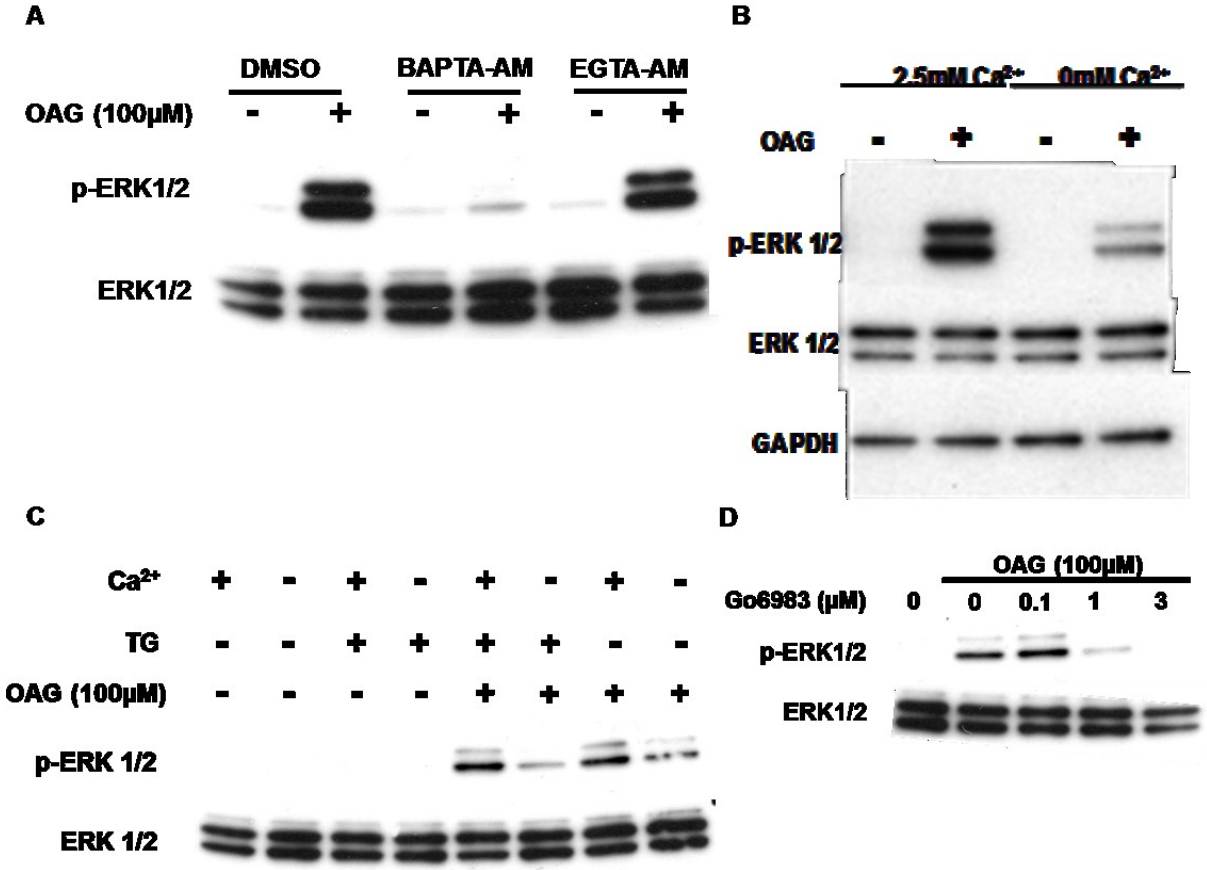

Figure 6

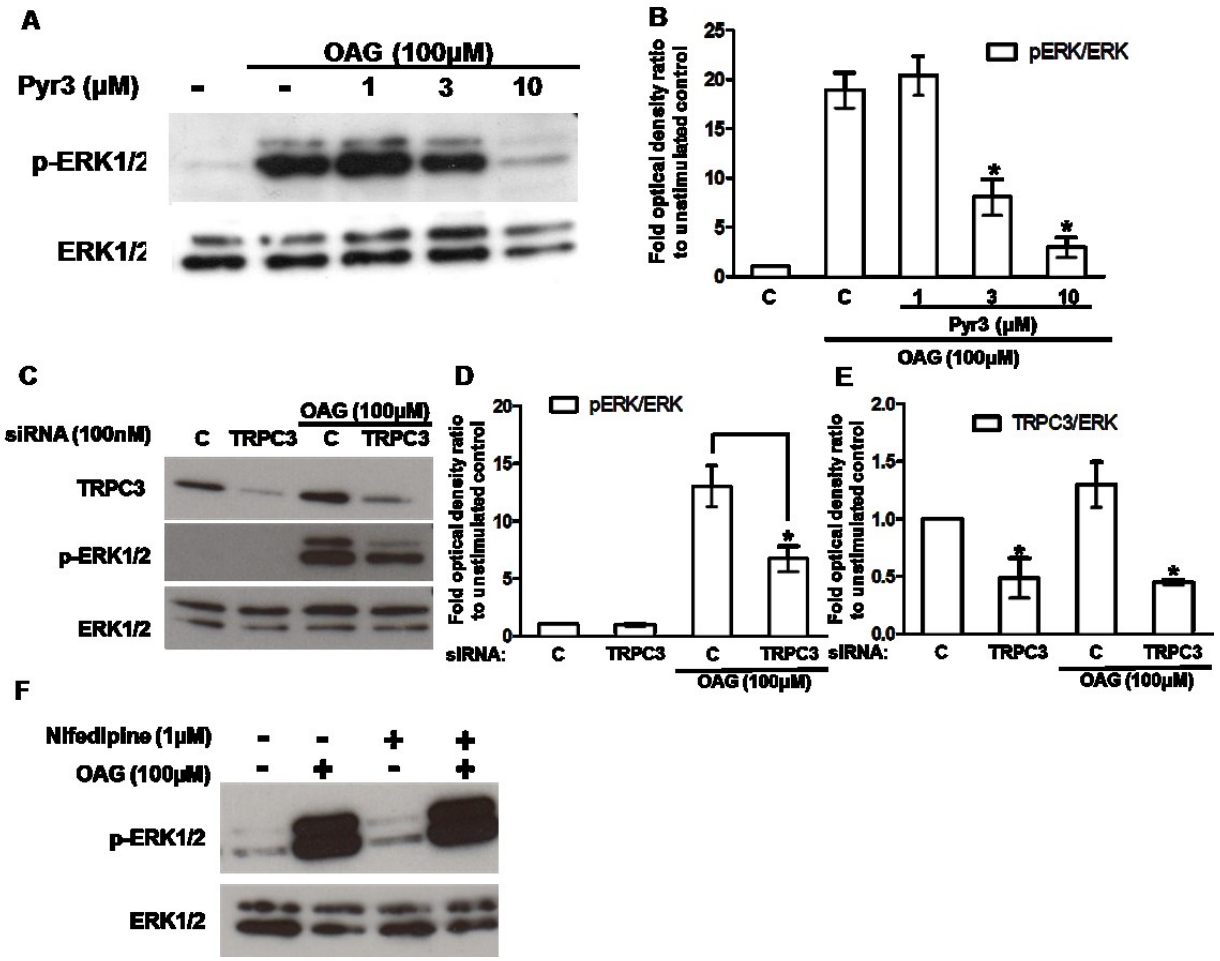
A
OAG (100μM)
Pyr3 (μM)
-
-
1
3
10
p-ERK1/2
ERK1/2
B
pERK/ERK
Fold optical density ratio to unstimulated control
C
C
1
3
10
Pyr3 (μM)
OAG (100μM)
C
siRNA (100nM)
C
TRPC3
C
TRPC3
OAG (100μM)
TRPC3
p-ERK1/2
ERK1/2
D
pERK/ERK
Fold optical density ratio to unstimulated control
siRNA:
C
TRPC3
C
TRPC3
OAG (100μM)
E
TRPC3/ERK
Fold optical density ratio to unstimulated control
siRNA:
C
TRPC3
C
TRPC3
OAG (100μM)
F
Nifedipine (1μM)
OAG (100μM)
p-ERK1/2
ERK1/2

Figure 7

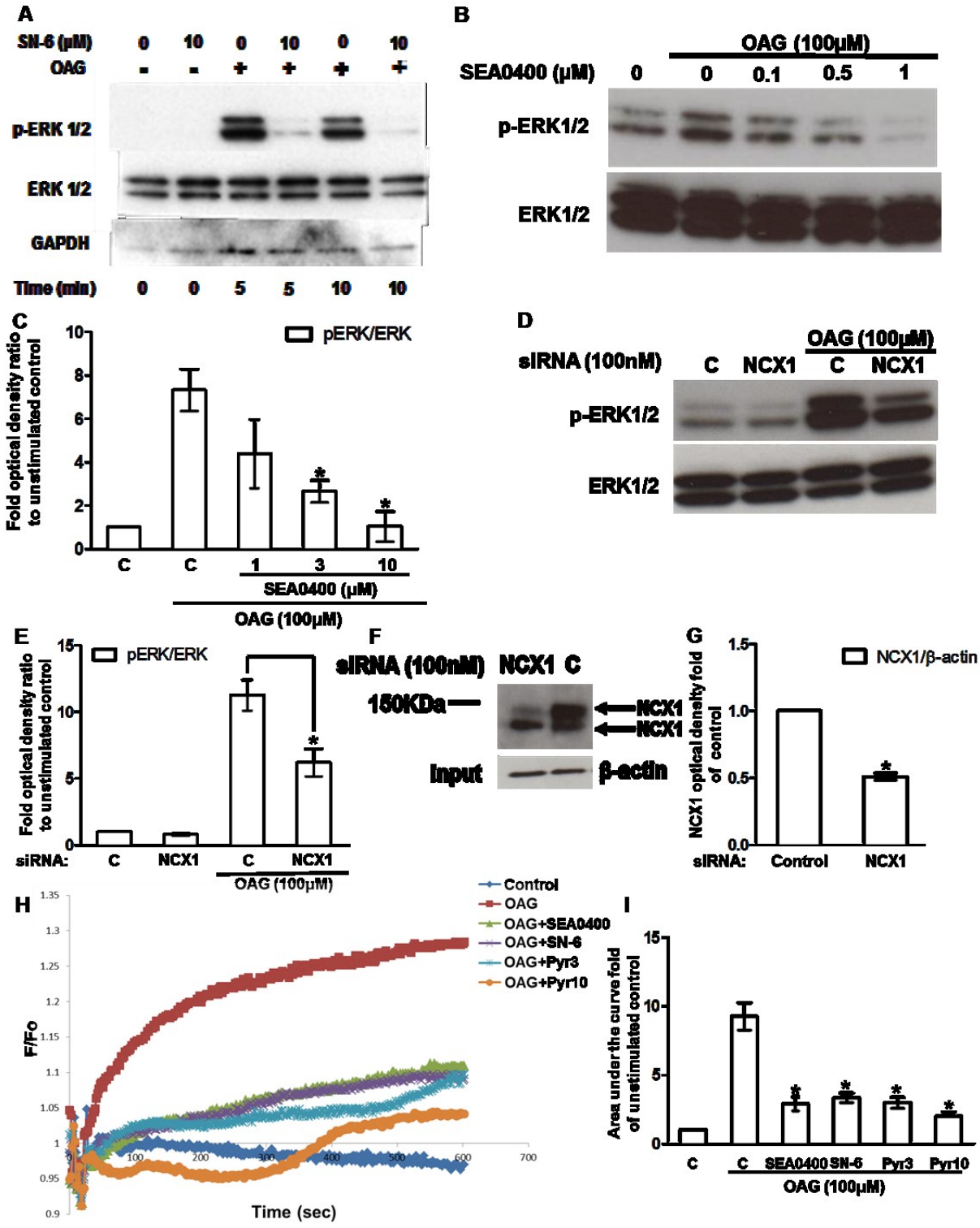
A
SN-6 (μM) 0 10 0 10 0 10
OAG - - + + + +
p-ERK 1/2
ERK 1/2
GAPDH
Time (min) 0 0 5 5 10 10
B
OAG (100μM)
SEA0400 (μM) 0 0 0.1 0.5 1
p-ERK1/2
ERK1/2
C
pERK/ERK
Fold optical density ratio to unstimulated control
C C 1 3 10
SEA0400 (μM)
OAG (100μM)
D
OAG (100μM)
siRNA (100nM) C NCX1 C NCX1
p-ERK1/2
ERK1/2
E
pERK/ERK
Fold optical density ratio to unstimulated control
siRNA: C NCX1 C NCX1
OAG (100μM)
F
siRNA (100nM) NCX1 C
150KDa
NCX1
NCX1
Input
β-actin
G
NCX1/β-actin
NCX1 optical density fold of control
siRNA: Control NCX1
H
Control
OAG
OAG+SEA0400
OAG+SN-6
OAG+Pyr3
OAG+Pyr10
F/Fo
Time (sec)
I
Area under the curve fold of unstimulated control
C C SEA0400 SN-6 Pyr3 Pyr10
OAG (100μM)

Figure 8

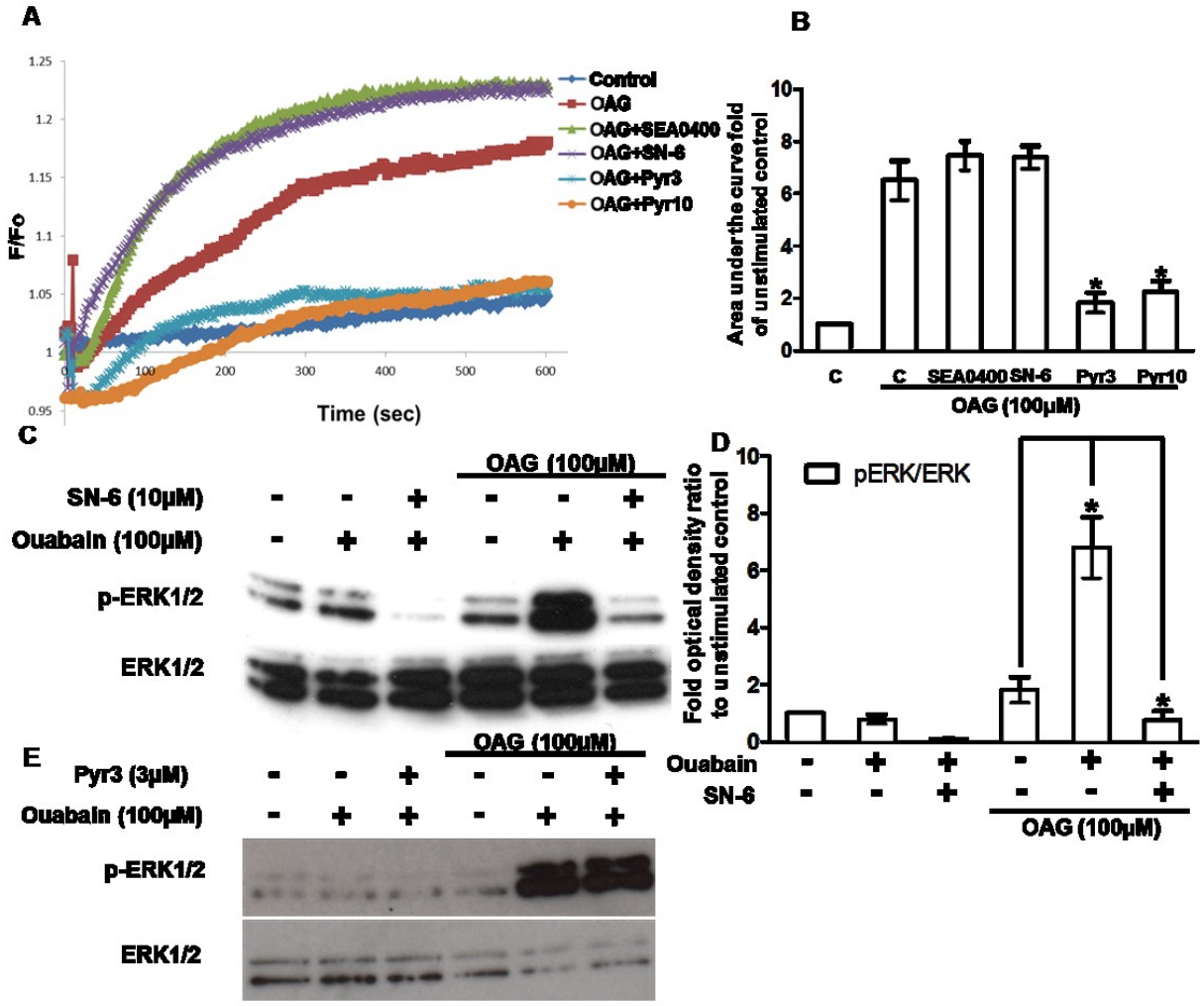
A
F/Fo
Time (sec)
Control
OAG
OAG+SEA0400
OAG+SN-6
OAG+Pyr3
OAG+Pyr10
B
Area under the curve fold of unstimulated control
C
SEA0400
SN-6
Pyr3
Pyr10
OAG (100μM)
C
SN-6 (10μM)
Ouabain (100μM)
p-ERK1/2
ERK1/2
OAG (100μM)
D
pERK/ERK
Fold optical density ratio to unstimulated control
Ouabain
SN-6
OAG (100μM)
E
Pyr3 (3μM)
Ouabain (100μM)
p-ERK1/2
ERK1/2
OAG (100μM)

Figure 9

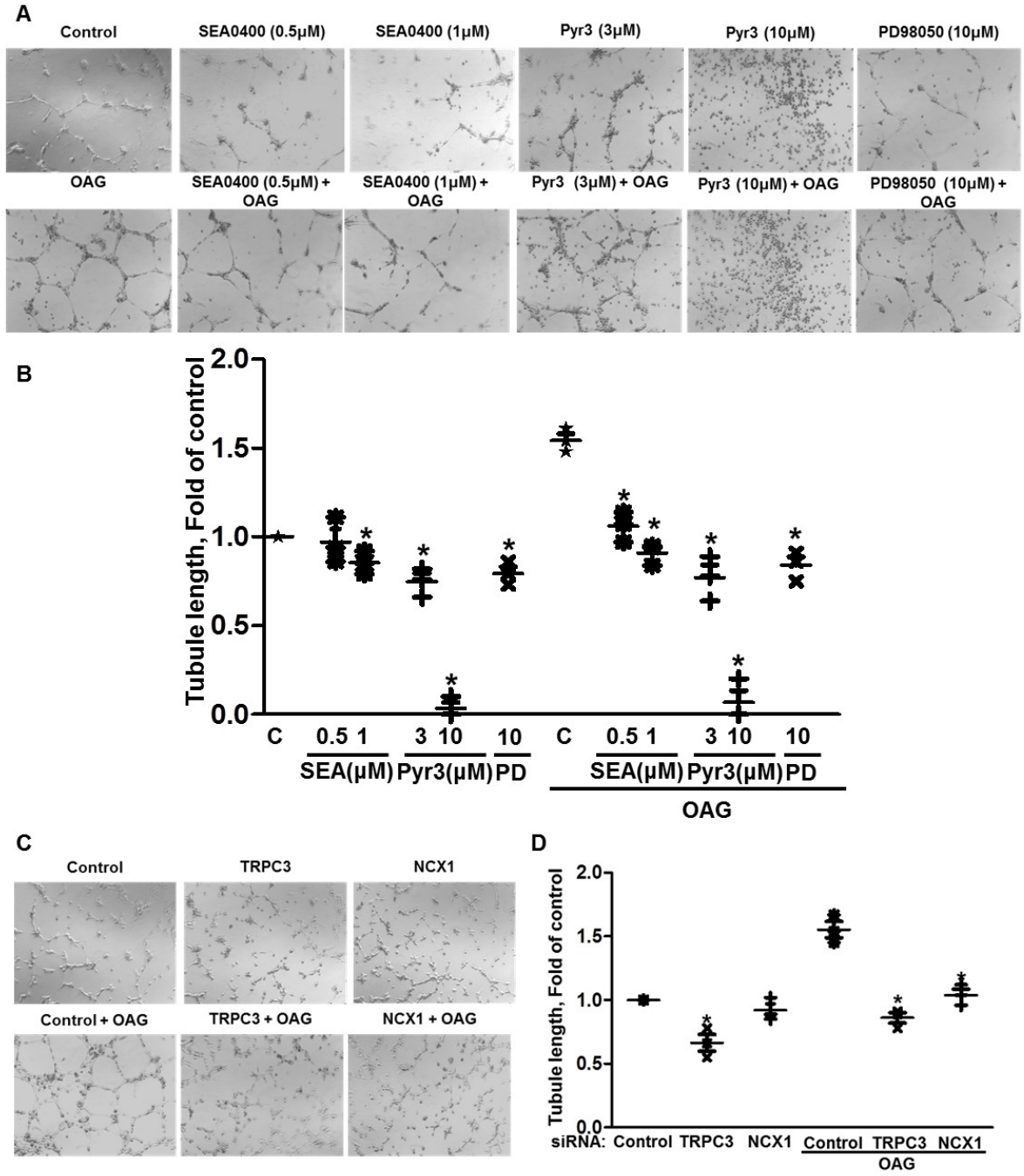
A
Control
SEA0400 (0.5μM)
SEA0400 (1μM)
Pyr3 (3μM)
Pyr3 (10μM)
PD98050 (10μM)
OAG
SEA0400 (0.5μM) + OAG
SEA0400 (1μM) + OAG
Pyr3 (3μM) + OAG
Pyr3 (10μM) + OAG
PD98050 (10μM) + OAG
B
Tubule length, Fold of control
2.0
1.5
1.0
0.5
0.0
C 0.5 1 3 10 10 C 0.5 1 3 10 10
SEA(μM) Pyr3(μM) PD SEA(μM) Pyr3(μM) PD
OAG
C
Control
TRPC3
NCX1
Control + OAG
TRPC3 + OAG
NCX1 + OAG
D
Tubule length, Fold of control
2.0
1.5
1.0
0.5
0.0
siRNA: Control TRPC3 NCX1 Control TRPC3 NCX1
OAG

Figure 10

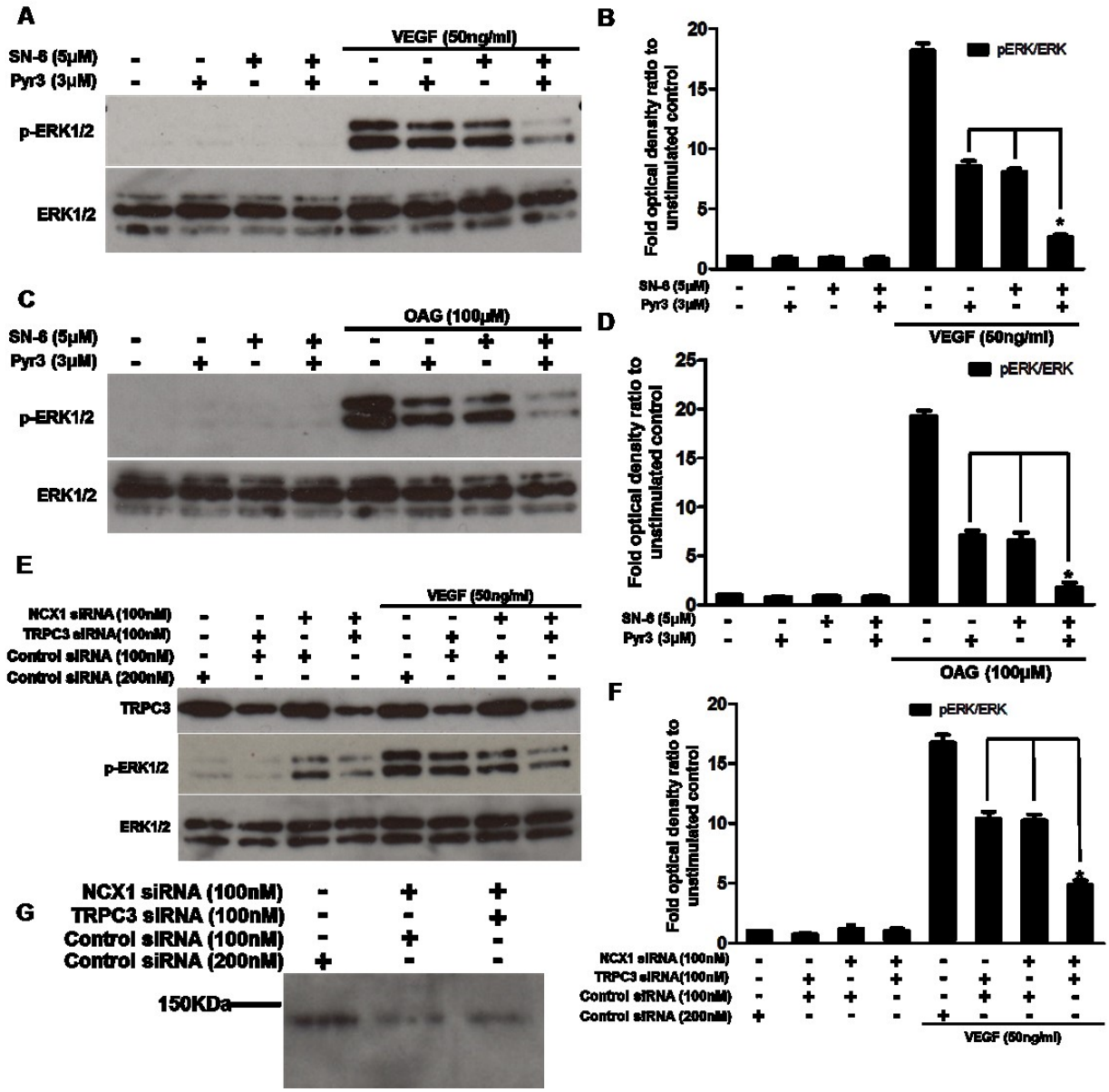
A
VEGF (50ng/ml)
SN-6 (5μM)
Pyr3 (3μM)
p-ERK1/2
ERK1/2
B
pERK/ERK
Fold optical density ratio to unstimulated control
SN-6 (5μM)
Pyr3 (3μM)
VEGF (50ng/ml)
C
OAG (100μM)
SN-6 (5μM)
Pyr3 (3μM)
p-ERK1/2
ERK1/2
D
pERK/ERK
Fold optical density ratio to unstimulated control
SN-6 (5μM)
Pyr3 (3μM)
OAG (100μM)
E
VEGF (50ng/ml)
NCX1 siRNA (100nM)
TRPC3 siRNA(100nM)
Control siRNA (100nM)
Control siRNA (200nM)
TRPC3
p-ERK1/2
ERK1/2
F
pERK/ERK
Fold optical density ratio to unstimulated control
NCX1 siRNA (100nM)
TRPC3 siRNA(100nM)
Control siRNA (100nM)
Control siRNA (200nM)
VEGF (50ng/ml)
G
NCX1 siRNA (100nM)
TRPC3 siRNA (100nM)
Control siRNA (100nM)
Control siRNA (200nM)
150KDa

Figure 11

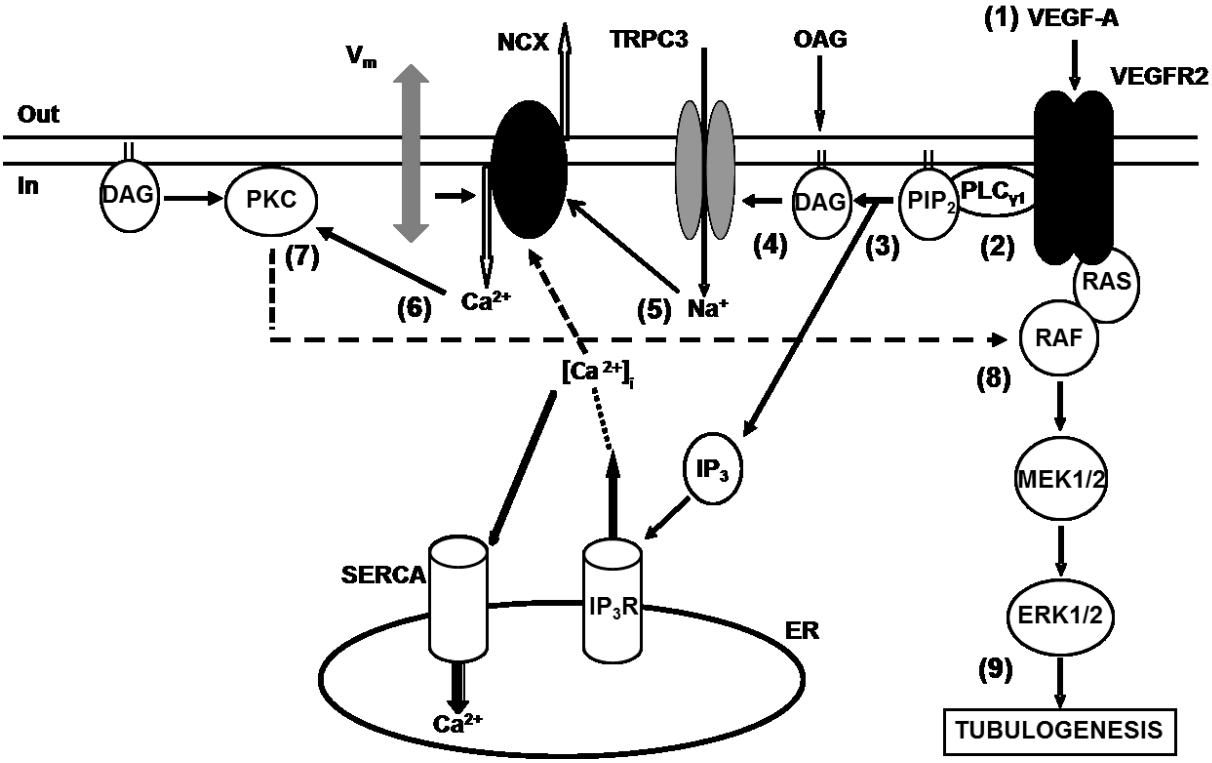
(1) VEGF-A
VEGFR2
NCX
TRPC3
OAG
V_m
Out
In
DAG
PKC
DAG
PIP_2
$PLC_{\gamma 1}$
(7)
(6)
Ca^{2+}
(5)
Na^+
(4)
(3)
(2)
RAS
RAF
(8)
$[Ca^{2+}]_i$
IP_3
MEK1/2
SERCA
IP_3R
ER
ERK1/2
Ca^{2+}
(9)
TUBULOGENESIS